

# Generalized Diffusion Model with Adjusted Offset Noise

Takuro Kutsuna\*

\*Toyota Central R&D Labs., Inc.

## Abstract

Diffusion models have become fundamental tools for modeling data distributions in machine learning and have applications in image generation, drug discovery, and audio synthesis. Despite their success, these models face challenges when generating data with extreme brightness values, as evidenced by limitations in widely used frameworks like Stable Diffusion. Offset noise has been proposed as an empirical solution to this issue, yet its theoretical basis remains insufficiently explored. In this paper, we propose a generalized diffusion model that naturally incorporates additional noise within a rigorous probabilistic framework. Our approach modifies both the forward and reverse diffusion processes, enabling inputs to be diffused into Gaussian distributions with arbitrary mean structures. We derive a loss function based on the evidence lower bound, establishing its theoretical equivalence to offset noise with certain adjustments, while broadening its applicability. Experiments on synthetic datasets demonstrate that our model effectively addresses brightness-related challenges and outperforms conventional methods in high-dimensional scenarios.

## 1 Introduction

One of the primary objectives of statistical machine learning is to model data distributions, a task that has supported recent advancements in generative artificial intelligence. The goal is to estimate a model that approximates an unknown distribution on the basis of multiple samples drawn from it. For example, when the data consists of images, the estimated model can be used to generate synthetic images that follow the same distribution.

Diffusion models [28, 11, 29, 14] have emerged as powerful tools for estimating probability distributions and generating new data samples. They have been shown to outperform other generative models, such as generative adversarial networks (GANs) [6], particularly in image generation tasks [5]. Due to their flexibility and effectiveness, diffusion models are now employed in a wide range of applications, including drug design [3, 8], audio synthesis [17], and text generation [1, 18].

A well-known challenge faced by diffusion models for image generation is their difficulty in producing images with extremely low or high brightness across the entire image [9, 19, 12]. For example, it has been reported that Stable Diffusion [26], a popular diffusion model for text-conditional image generation, struggles to generate fully black or fully white images when given prompts such as "Solid black image" or "A white background" [19].<sup>1</sup>

Offset noise [9] has been proposed as a solution to this issue and has been empirically demonstrated to be effective; however, its theoretical foundation remains unclear. Specifically, offset noise introduces additional noise  $\epsilon_c \sim q(\epsilon_c)$ , which is correlated across image channels, into the standard normal noise used during the training of denoising diffusion models [11]. Experiments have demonstrated that offset noise effectively mitigates brightness-related issues, and this technique has been incorporated in widely used models, such as SDXL [25], a successor to Stable Diffusion. Nevertheless, the theoretical justification for introducing  $\epsilon_c$  during

<sup>1</sup>The study in [19] uses Stable Diffusion 2.1-base.

training remains ambiguous, raising concerns that the use of offset noise may diverge from the well-established theoretical framework of the original diffusion models.<sup>2</sup>

In this study, we propose a novel diffusion model whose training loss function, derived from the evidence lower bound, takes a similar form to the loss function with offset noise, with certain adjustments. The proposed model modifies the forward and reverse processes of the original discrete-time diffusion models [28, 11] to naturally incorporate additional noise  $\xi \sim q(\xi)$ , which corresponds to  $\epsilon_c$  in offset noise. The key difference between the loss function of the proposed model and that of the offset noise model lies in the treatment of the additional noise. In the proposed model, the noise is multiplied by time-dependent coefficients before being added to the standard normal noise  $\epsilon$ . In contrast to offset noise, the proposed model is grounded in a well-defined probabilistic framework, ensuring theoretical compatibility with other methods for diffusion models. In particular, we explore its integration with the  $v$ -prediction framework [27].

Another feature of the proposed model is that, unlike conventional diffusion models where any input is diffused into standard Gaussian noise  $\mathcal{N}(0, I)$  with zero mean, the proposed model diffuses any input to  $\mathcal{N}(\xi, I)q(\xi)$  through the forward process. In the reverse process, a new sample is generated starting from the initial distribution  $\mathcal{N}(\xi, I)q(\xi)$ . Since the distribution  $q(\xi)$  can be specified as an arbitrary distribution, the proposed model allows inputs to be diffused into a Gaussian distribution with any desired mean structure and generates new samples from that distribution. If we set  $q(\xi)$  as a Dirac delta function at  $\xi = 0$ , the proposed model reduces to the conventional diffusion model, indicating that it includes the original diffusion models as a special case.

In summary, the contributions of this study are as follows:

- We propose a diffusion model that derives a loss function similar to that of the offset noise model, with certain adjustments. The key difference between the two loss functions is that, in the proposed model, the additional noise is multiplied by time-dependent coefficients before being added to the standard normal noise. (Theorem 3.1)
- The proposed model generalizes conventional diffusion models by diffusing its inputs into Gaussian distributions with arbitrary mean structures, including the original zero-mean Gaussian distribution as a special case. (Proposition 3.2)
- Because the proposed model is grounded in a well-defined probabilistic framework, in contrast to the offset noise model, it ensures theoretical compatibility with other methods for diffusion models. In particular, we discuss its integration with  $v$ -prediction [27]. (section 5)
- We empirically demonstrate the superiority of the proposed model by using a synthetic dataset that simulates a scenario where image brightness is uniformly distributed from solid black and pure white. This scenario is shown to be less effectively modeled by conventional diffusion models, especially in high-dimensional data settings, whereas the proposed model successfully generates data that follows the true distribution. (section 7)

## 2 Preliminary

In this section, we provide a summary of the aspects of diffusion models that are relevant to our research.

### 2.1 Diffusion models

Diffusion models learn the distribution of observed data and enable sampling of new data from the learned distribution. These models have been developed for both discrete-time [28, 11] and continuous-time [29, 14] frameworks; in this study, we focus on discrete-time models.

---

<sup>2</sup>For example, Lin et al. [19] states that “(offset noise) is incongruent with the theory of the diffusion process,” while Hu et al. [12] refers to offset noise as “an unprincipled ad hoc adjustment.”

### 2.1.1 Forward and reverse processes

Let  $\mathbf{x}_0 \in \mathbb{R}^n$  represent data<sup>3</sup> sampled from the probability distribution  $p_{\text{gt}}(\mathbf{x}_0)$ . Diffusion models define two processes: the forward process, which gradually adds noise to  $\mathbf{x}_0$ , and the reverse process, which removes noise. The forward process is defined as follows:

$$q(\mathbf{x}_{1:T}|\mathbf{x}_0) = \prod_{t=1}^T q(\mathbf{x}_t|\mathbf{x}_{t-1}), \quad (1)$$

$$q(\mathbf{x}_t|\mathbf{x}_{t-1}) = \mathcal{N}\left(\mathbf{x}_t \mid \sqrt{1 - \beta_t}\mathbf{x}_{t-1}, \beta_t I\right) \text{ for } t = 1, \dots, T, \quad (2)$$

where  $\mathbf{x}_t \in \mathbb{R}^n$  ( $t = 1, \dots, T$ ) represents the intermediate variables during the diffusion process, and  $\mathbf{x}_{1:T} = (\mathbf{x}_1, \dots, \mathbf{x}_T)$ . The parameters  $\beta_t > 0$  ( $t = 1, \dots, T$ ) are pre-determined variance scheduling parameters. Here,  $\mathcal{N}(\mathbf{a} \mid \boldsymbol{\mu}, \Sigma)$  denotes the probability density function of a normal distribution for the random variable  $\mathbf{a}$  with mean  $\boldsymbol{\mu}$  and variance-covariance matrix (hereafter simply referred to as variance)  $\Sigma$ , and  $I$  represents the  $n \times n$  identity matrix. Starting from data  $\mathbf{x}_0 \sim p_{\text{gt}}(\mathbf{x}_0)$ , the forward process sequentially generates  $\mathbf{x}_t$  from a normal distribution with mean and variance determined by  $\mathbf{x}_{t-1}$  and  $\beta_t$ . With appropriately chosen values of  $\beta_t$ ,  $\mathbf{x}_T$  converges to a normal distribution with mean 0 and variance  $I$ . This implies that, after  $T$  steps, any  $\mathbf{x}_0$  will diffuse into pure noise, containing no information about  $\mathbf{x}_0$ . Note that the forward process does not include any learnable parameters.

The reverse process is defined as follows:

$$p_{\theta}(\mathbf{x}_{0:T}) = p(\mathbf{x}_T) \prod_{t=1}^T p_{\theta}(\mathbf{x}_{t-1}|\mathbf{x}_t), \quad (3)$$

$$p(\mathbf{x}_T) = \mathcal{N}(\mathbf{x}_T \mid 0, I), \quad (4)$$

$$p_{\theta}(\mathbf{x}_{t-1}|\mathbf{x}_t) = \mathcal{N}(\mathbf{x}_{t-1} \mid \mu_{\theta}(\mathbf{x}_t, t), \sigma_t^2 I) \text{ for } t = 1, \dots, T, \quad (5)$$

where  $\mu_{\theta}$  is the function with parameter  $\theta$  learned in the diffusion model, representing the mean of the normal distribution used to generate  $\mathbf{x}_{t-1}$  from  $\mathbf{x}_t$ . In the reverse process,  $\mathbf{x}_T$  is initially generated as pure noise, after which the mean of  $\mathbf{x}_{T-1}$  is predicted by  $\mu_{\theta}$  using  $\mathbf{x}_T$  and the time step  $T$ . Subsequently,  $\mathbf{x}_{T-1}$  is generated according to (5). This process is repeated similarly for each time step down to  $t = 1$ , eventually yielding  $\mathbf{x}_0$ . While it is possible to consider the variance  $\sigma_t^2$  in (5) as a learnable parameter, it has been shown that setting  $\sigma_t^2 = \beta_t$  provides sufficiently high performance [11]. Therefore, we will exclude it from the learnable parameters.

### 2.1.2 Training procedure

To learn the parameter  $\theta$  discussed in the previous section, diffusion models aim to maximize the log-likelihood  $\log p_{\theta}(\mathbf{x}_0)$  given the data  $\mathbf{x}_0$ . If we could marginalize over  $\mathbf{x}_{1:T}$  in (3), we would be able to directly evaluate  $\log p_{\theta}(\mathbf{x}_0)$ ; however, this computation is highly complex. Therefore, diffusion models typically instead derive the following evidence lower bound, and they learn  $\theta$  by maximizing this bound.

$$\log p_{\theta}(\mathbf{x}_0) \geq \mathbb{E}_{q(\mathbf{x}_{1:T}|\mathbf{x}_0)} \left[ \log \frac{p_{\theta}(\mathbf{x}_{0:T})}{q(\mathbf{x}_{1:T}|\mathbf{x}_0)} \right] \quad (6)$$

Note that in (6), the model for the reverse process appears in the numerator on the right-hand side, while the model for the forward process appears in the denominator. In deriving the above evidence lower bound, all intermediate variables  $\mathbf{x}_{1:T}$  are treated as latent variables, with the forward process model serving as an approximate posterior distribution for the latent variables conditioned on  $\mathbf{x}_0$ .

<sup>3</sup>When  $\mathbf{x}_0$  represents an image, it typically has a structure consisting of color channels, which have a width and height, but here we assume a generalized vector form. For instance, even image data can be treated as vector data by flattening its elements into a single column.

Under the models for the forward and reverse processes discussed in the previous section, the loss function for maximizing the right-hand side of (6) is derived as follows [11, 22]:

$$\hat{\ell}(\theta; \mathbf{x}_0) = \mathbb{E}_{\mathcal{U}(t|1,T), q(\mathbf{x}_t|\mathbf{x}_0)} \left[ \frac{1}{2\sigma_t^2} \|\tilde{\mu}_t(\mathbf{x}_t, \mathbf{x}_0) - \mu_\theta(\mathbf{x}_t, t)\|^2 \right], \quad (7)$$

where  $\mathcal{U}(t | 1, T)$  denotes the discrete uniform distribution over  $\{1, \dots, T\}$ ,  $\tilde{\mu}_t(\mathbf{x}_t, \mathbf{x}_0)$  represents the analytically derived target mean, and  $\|\cdot\|$  denotes the 2-norm of a vector. Note that, due to the reproductive property of the normal distribution,  $q(\mathbf{x}_t|\mathbf{x}_0)$  is also a normal distribution, which simplifies the computation of expectations with respect to  $\mathbf{x}_t$ .

### 2.1.3 Denoising modeling

Instead of directly predicting  $\tilde{\mu}_t$  with  $\mu_\theta$  as in (7), DDPM [11] assumes the following form for  $\mu_\theta$ :

$$\mu_\theta(\mathbf{x}_t, t) = \frac{1}{\sqrt{\alpha_t}} \mathbf{x}_t - \frac{1 - \alpha_t}{\sqrt{1 - \bar{\alpha}_t} \sqrt{\alpha_t}} \epsilon_\theta(\mathbf{x}_t, t), \quad (8)$$

where  $\alpha_t$  and  $\bar{\alpha}_t$  are constants determined by  $\beta_t$  (details will be provided in subsection 3.2). In this model, the objective is to learn  $\epsilon_\theta(\mathbf{x}_t, t)$  instead of  $\mu_\theta(\mathbf{x}_t, t)$ . Consequently, the loss function in (7) can be reformulated as follows [11] (excluding terms that do not depend on  $\theta$ ):

$$\hat{\ell}(\theta; \mathbf{x}_0) = \mathbb{E}_{\mathcal{U}(t|1,T), \mathcal{N}(\epsilon_0|0,I)} \left[ \lambda_t \|\epsilon_0 - \epsilon_\theta(\mathbf{x}_t, t)\|^2 \right] \quad (9)$$

$$= \mathbb{E}_{\mathcal{U}(t|1,T), \mathcal{N}(\epsilon_0|0,I)} \left[ \lambda_t \|\epsilon_0 - \epsilon_\theta(\sqrt{\bar{\alpha}_t} \mathbf{x}_0 + \sqrt{1 - \bar{\alpha}_t} \epsilon_0, t)\|^2 \right], \quad (10)$$

where  $\lambda_t$  is given by

$$\lambda_t = \frac{(1 - \alpha_t)^2}{2\sigma_t^2 \alpha_t (1 - \bar{\alpha}_t)}. \quad (11)$$

From (9) to (10), we have used the relationship  $\mathbf{x}_t = \sqrt{\bar{\alpha}_t} \mathbf{x}_0 + \sqrt{1 - \bar{\alpha}_t} \epsilon_0$ , which follows from  $q(\mathbf{x}_t|\mathbf{x}_0)$ . Research has shown that by modeling  $\epsilon_\theta$  instead of  $\mu_\theta$  as the learning target, the training of diffusion models becomes more efficient [11]. Moreover, experimental results suggest that using the simplified loss function below, where the  $\lambda_t$  in (10) are set to 1, achieves better performance compared with directly using (10) as the loss function [11]:

$$\hat{\ell}_{\text{simple}}(\theta; \mathbf{x}_0) = \mathbb{E}_{\mathcal{U}(t|1,T), \mathcal{N}(\epsilon_0|0,I)} \left[ \|\epsilon_0 - \epsilon_\theta(\sqrt{\bar{\alpha}_t} \mathbf{x}_0 + \sqrt{1 - \bar{\alpha}_t} \epsilon_0, t)\|^2 \right] \quad (12)$$

## 2.2 Offset noise

One problem with diffusion models, particularly when  $\mathbf{x}_0$  represents an image, is that they are less likely to generate images with extremely low or high overall brightness [9, 19, 12]. One way to address this issue is to use offset noise [9]. In the offset noise method, the following loss function replaces the loss function in (12):

$$\hat{\ell}_{\text{offset}}(\theta; \mathbf{x}_0) = \mathbb{E}_{\mathcal{U}(t|1,T), \mathcal{N}(\epsilon_0|0,I), q(\epsilon_c)} \left[ \|\epsilon_0 + \epsilon_c - \epsilon_\theta(\sqrt{\bar{\alpha}_t} \mathbf{x}_0 + \sqrt{1 - \bar{\alpha}_t} (\epsilon_0 + \epsilon_c), t)\|^2 \right] \quad (13)$$

Compared with (12), an additional noise term  $\epsilon_c \sim q(\epsilon_c)$  is added to  $\epsilon_0$  in (13), where  $q(\epsilon_c)$  is a zero-mean normal distribution with fully correlated variance across image channels. Formally,  $q(\epsilon_c)$  is expressed as  $q(\epsilon_c) = \mathcal{N}(\epsilon_c | 0, \sigma_c^2 \Sigma_c)$ , where  $\Sigma_c$  is a block-diagonal matrix with off-diagonal elements of 1 within each channel, and  $\sigma_c^2$  is a parameter that controls the intensity of the offset noise.

An intuitive explanation as to why diffusion models have difficulty generating images with extreme brightness and why offset noise can mitigate this issue is discussed in [9], as follows: In the forward process of

diffusion models, noise is gradually added to  $\mathbf{x}_0$ , assuming that  $\mathbf{x}_T$  will have ideally diffused into pure Gaussian noise by the final time step  $T$ . However, in actual numerical calculations,  $\mathbf{x}_T$  does not fully become pure Gaussian noise in the forward process; specifically, lower-frequency components of  $\mathbf{x}_0$  tend to remain in  $\mathbf{x}_T$ . Since images with overall low or high brightness contain stronger low-frequency components,  $\mathbf{x}_T$  for these images tends to deviate significantly from pure Gaussian noise. Nonetheless, in the reverse process,  $\mathbf{x}_T$  is pure Gaussian noise according to (4) and is used as the initial condition to generate  $\mathbf{x}_0$ . As a result, images with low or high brightness are less likely to be generated. On the basis of this consideration, [9] proposes adding offset noise as a way to effectively diffuse the low-frequency components contained in  $\mathbf{x}_0$ . Experiments have demonstrated that incorporating offset noise during training enables diffusion models to generate images with low or high brightness [9]. Consequently, offset noise has been used to train widely-used diffusion models, including SDXL [25] and Illuminati Diffusion [13].

However, it remains unclear how the loss function in (13) modifies the original forward and reverse processes used by diffusion models. Such issues pose a challenge to integrating offset noise with other techniques in diffusion models. In this regard, it is important to investigate a probabilistic interpretation of the offset noise model.

### 3 Proposed model

We will begin by defining the forward and reverse processes for the proposed model and then derive a loss function based on the evidence lower bound of its log-likelihood. We will show that the resulting loss function takes a similar form to that of the offset noise model, differing only in the coefficients of the additional noise.

#### 3.1 Forward and reverse processes

The forward process in the proposed model is defined as follows:

$$q(\mathbf{x}_{1:T}, \boldsymbol{\xi} | \mathbf{x}_0) = q(\boldsymbol{\xi}) \prod_{t=1}^T q(\mathbf{x}_t | \mathbf{x}_{t-1}, \boldsymbol{\xi}), \quad (14)$$

$$q(\mathbf{x}_t | \mathbf{x}_{t-1}, \boldsymbol{\xi}) = \mathcal{N} \left( \mathbf{x}_t \mid \sqrt{1 - \beta_t} (\mathbf{x}_{t-1} + \gamma_t \boldsymbol{\xi}), \beta_t \sigma_0^2 I \right) \text{ for } t = 1, \dots, T, \quad (15)$$

where  $\boldsymbol{\xi} \in \mathbb{R}^n$  is a newly introduced random variable, with  $q(\boldsymbol{\xi})$  representing its probability density function. Note that  $\boldsymbol{\xi}$  is independent of time  $t$ . Moreover, we do not assume a specific form for  $q(\boldsymbol{\xi})$  and allow  $\boldsymbol{\xi}$  to follow any arbitrary distribution. A scalar parameter  $\sigma_0 \in \mathbb{R}$  is introduced as a scaling factor for the variance. Additionally,  $\gamma_t \in \mathbb{R}$  ( $t = 1, \dots, T$ ) is introduced as a coefficient of  $\boldsymbol{\xi}$ , and it plays an important role in determining the coefficients of the additional noise in the loss function for the proposed model, as will be explained in the next section. The construction of  $\gamma_t$  will be discussed in section 4.

The reverse process in the proposed model is defined as follows:

$$p_\theta(\mathbf{x}_{0:T}, \boldsymbol{\xi}) = p(\boldsymbol{\xi}) p(\mathbf{x}_T | \boldsymbol{\xi}) \prod_{t=1}^T p_\theta(\mathbf{x}_{t-1} | \mathbf{x}_t), \quad (16)$$

$$p(\boldsymbol{\xi}) = q(\boldsymbol{\xi}), \quad (17)$$

$$p(\mathbf{x}_T | \boldsymbol{\xi}) = \mathcal{N}(\mathbf{x}_T \mid \boldsymbol{\xi}, \sigma_0^2 I), \quad (18)$$

$$p_\theta(\mathbf{x}_{t-1} | \mathbf{x}_t) = \mathcal{N}(\mathbf{x}_{t-1} \mid \mu_\theta(\mathbf{x}_t, t), \sigma_t^2 I) \text{ for } t = 1, \dots, T. \quad (19)$$

The main difference between the proposed reverse process and the original reverse process in (3)–(5) is that the mean of  $\mathbf{x}_T$  is changed from 0 to  $\boldsymbol{\xi}$ . Note that  $p_\theta(\mathbf{x}_{t-1} | \mathbf{x}_t)$  in (19) remains equivalent to that in (5).

### 3.2 Main results: loss function for the proposed model

We define  $\alpha_0 = 1$ ,  $\alpha_t = 1 - \beta_t$  ( $t = 1, \dots, T$ ), and  $\bar{\alpha}_t = \prod_{i=0}^t \alpha_i$ .<sup>4</sup> Given the forward and reverse processes defined in the previous section, the loss function for training the proposed model is derived from the evidence lower bound of the log-likelihood as follows:

**Theorem 3.1** (Training loss function). *Suppose the forward process is defined as in (14) and (15) and the reverse process is as in (16)–(19). Accordingly, the loss function that maximizes the evidence lower bound of  $\log p_\theta(\mathbf{x}_0)$  is given by*

$$\ell(\theta; \mathbf{x}_0) = \mathbb{E}_{q(\boldsymbol{\xi}), \mathcal{U}(t|1, T), \mathcal{N}(\boldsymbol{\epsilon}_0|0, I)} \left[ \lambda_t \left\| \sigma_0 \boldsymbol{\epsilon}_0 + \phi_t \boldsymbol{\xi} - \epsilon_\theta \left( \sqrt{\bar{\alpha}_t} \mathbf{x}_0 + \sqrt{1 - \bar{\alpha}_t} (\sigma_0 \boldsymbol{\epsilon}_0 + \psi_t \boldsymbol{\xi}), t \right) \right\|^2 \right], \quad (20)$$

where  $\lambda_t$  is given by (11), and  $\phi_t$  and  $\psi_t$  are given by

$$\phi_t = \frac{\sqrt{\bar{\alpha}_t} \sqrt{1 - \bar{\alpha}_t}}{1 - \alpha_t} \gamma_t \text{ for } t = 1, \dots, T, \quad (21)$$

$$\psi_t = \frac{1}{\sqrt{1 - \bar{\alpha}_t}} \sum_{i=1}^t \sqrt{\frac{\bar{\alpha}_t}{\bar{\alpha}_{i-1}}} \gamma_i \text{ for } t = 1, \dots, T. \quad (22)$$

In the following subsections, we provide a detailed derivation of the loss function in Theorem 3.1.

#### 3.2.1 Evidence lower bound

The evidence lower bound for the proposed model decomposes into three terms:

$$\begin{aligned} \log p_\theta(\mathbf{x}_0) &\geq \mathbb{E}_{q(\mathbf{x}_{1:T}, \boldsymbol{\xi} | \mathbf{x}_0)} \left[ \log \frac{p_\theta(\mathbf{x}_{0:T}, \boldsymbol{\xi})}{q(\mathbf{x}_{1:T}, \boldsymbol{\xi} | \mathbf{x}_0)} \right] \\ &= \underbrace{\mathbb{E}_{q(\boldsymbol{\xi})} \mathbb{E}_{q(\mathbf{x}_1 | \mathbf{x}_0, \boldsymbol{\xi})} [\log p_\theta(\mathbf{x}_0 | \mathbf{x}_1)]}_{\mathcal{L}_1} - \underbrace{\mathbb{E}_{q(\boldsymbol{\xi})} [D_{\text{KL}}(q(\mathbf{x}_T | \mathbf{x}_0, \boldsymbol{\xi}) || p(\mathbf{x}_T | \boldsymbol{\xi}))]}_{\mathcal{L}_2} \\ &\quad - \underbrace{\sum_{t=2}^T \mathbb{E}_{q(\boldsymbol{\xi})} \mathbb{E}_{q(\mathbf{x}_t | \mathbf{x}_0, \boldsymbol{\xi})} [D_{\text{KL}}(q(\mathbf{x}_{t-1} | \mathbf{x}_t, \mathbf{x}_0, \boldsymbol{\xi}) || p_\theta(\mathbf{x}_{t-1} | \mathbf{x}_t))]}_{\mathcal{L}_3}, \end{aligned} \quad (23)$$

where  $D_{\text{KL}}(\cdot || \cdot)$  denotes the Kullback-Leibler (KL) divergence. See Appendix A.1 for a detailed derivation of (23). We refer to the first, second, and third terms in (23) as  $\mathcal{L}_1$ ,  $\mathcal{L}_2$ , and  $\mathcal{L}_3$ , respectively. In the following, we discuss each term in the order  $\mathcal{L}_2$ ,  $\mathcal{L}_3$ , and  $\mathcal{L}_1$ .

#### 3.2.2 $\mathcal{L}_2$

Since  $\mathcal{L}_2$  does not depend on  $\theta$ , it can be ignored during the optimization of  $\theta$ . Note that the value of  $\mathcal{L}_2$  increases as the distribution of  $\mathbf{x}_T$  obtained from the forward process aligns more closely with the distribution of  $\mathbf{x}_T$  in the reverse process. It can be shown that these distributions coincide under appropriate settings of  $\beta_t$  and  $\gamma_t$  in the proposed model (see Proposition 3.2). Therefore, under such settings,  $\mathcal{L}_2$  in the proposed model is guaranteed to reach its optimal value of zero.

<sup>4</sup>In standard diffusion models [11],  $\alpha_0$  is not defined, but here we introduce  $\alpha_0 = 1$  for convenience in our derivations. Consequently, the definition of  $\bar{\alpha}_t$  differs from the conventional one ( $\prod_{i=1}^t \alpha_i$ ); however, since  $\alpha_0 = 1$ , this modified  $\bar{\alpha}_t$  is essentially equivalent to the standard  $\bar{\alpha}_t$ .

### 3.2.3 Derivation of $\mathcal{L}_3$

**Derivation of  $q(\mathbf{x}_t|\mathbf{x}_0, \boldsymbol{\xi})$**  The variable  $\mathbf{x}_t$  ( $t = 1, \dots, T$ ), which follows  $q(\mathbf{x}_t|\mathbf{x}_0, \boldsymbol{\xi})$  in  $\mathcal{L}_3$ , can be expressed as follows:

$$\mathbf{x}_t = \sqrt{\bar{\alpha}_t}\mathbf{x}_0 + \sqrt{1 - \bar{\alpha}_t}(\sigma_0\boldsymbol{\epsilon}_0 + \psi_t\boldsymbol{\xi}), \quad (24)$$

where  $\boldsymbol{\epsilon}_0 \sim \mathcal{N}(\boldsymbol{\epsilon}_0 | 0, I)$  and  $\psi_t$  ( $t = 1, \dots, T$ ) is given by (22). See Appendix A.2 for a detailed derivation of (24). From (24), the distribution of  $\mathbf{x}_t$  in the forward process, given  $\mathbf{x}_0$  and  $\boldsymbol{\xi}$ , can be expressed as follows by using the reparameterization trick [15].

$$q(\mathbf{x}_t|\mathbf{x}_0, \boldsymbol{\xi}) = \mathcal{N}(\mathbf{x}_t | \sqrt{\bar{\alpha}_t}\mathbf{x}_0 + \sqrt{1 - \bar{\alpha}_t}\psi_t\boldsymbol{\xi}, (1 - \bar{\alpha}_t)\sigma_0^2I) \quad (25)$$

From (25), the following proposition holds:

**Proposition 3.2.** *Suppose  $\bar{\alpha}_t \rightarrow 0$  and  $\psi_t \rightarrow 1$  as  $t \rightarrow T$ . Then, it holds that  $q(\mathbf{x}_t|\mathbf{x}_0, \boldsymbol{\xi}) \rightarrow \mathcal{N}(\mathbf{x}_T | \boldsymbol{\xi}, \sigma_0^2I)$ .*

Proposition 3.2 states that, in the proposed model, any input  $\mathbf{x}_0$  will have diffused into a normal distribution with mean  $\boldsymbol{\xi}$  and variance  $\sigma_0^2I$  by the final time step.

**Derivation of  $q(\mathbf{x}_{t-1}|\mathbf{x}_t, \mathbf{x}_0, \boldsymbol{\xi})$**  The term  $q(\mathbf{x}_{t-1}|\mathbf{x}_t, \mathbf{x}_0, \boldsymbol{\xi})$  ( $t = 2, \dots, T$ ) can be derived as follows:

$$q(\mathbf{x}_{t-1}|\mathbf{x}_t, \mathbf{x}_0, \boldsymbol{\xi}) = \mathcal{N}(\mathbf{x}_{t-1} | \tilde{\mu}_t(\mathbf{x}_t, \mathbf{x}_0, \boldsymbol{\xi}), \tilde{\beta}_tI), \quad (26)$$

$$\tilde{\mu}_t(\mathbf{x}_t, \mathbf{x}_0, \boldsymbol{\xi}) = \frac{\sqrt{\bar{\alpha}_t}(1 - \bar{\alpha}_{t-1})}{1 - \bar{\alpha}_t}\mathbf{x}_t + \frac{(1 - \alpha_t)\sqrt{\bar{\alpha}_{t-1}}}{1 - \bar{\alpha}_t}\mathbf{x}_0 + \nu_t\boldsymbol{\xi}, \quad (27)$$

$$\tilde{\beta}_t = \frac{(1 - \alpha_t)(1 - \bar{\alpha}_{t-1})}{1 - \bar{\alpha}_t}\sigma_0^2, \quad (28)$$

where  $\nu_t$  ( $t = 2, \dots, T$ ) is given by

$$\nu_t = \frac{(1 - \alpha_t)\sqrt{1 - \bar{\alpha}_{t-1}}\psi_{t-1} - \alpha_t(1 - \bar{\alpha}_{t-1})\gamma_t}{1 - \bar{\alpha}_t}. \quad (29)$$

See Appendix A.3 for a detailed derivation of (26)–(29). When  $\gamma_t$  is determined using the method described in section 4, it can be shown that  $\nu_t = 0$  ( $t = 2, \dots, T$ ). Under this condition, and with the additional assumption that  $\sigma_0 = 1$ , the conditional distribution  $q(\mathbf{x}_{t-1}|\mathbf{x}_t, \mathbf{x}_0, \boldsymbol{\xi})$  reduces to  $q(\mathbf{x}_{t-1}|\mathbf{x}_t, \mathbf{x}_0)$  as defined in standard diffusion models [11], as detailed in Proposition 4.1.

**Towards denoising modeling** To apply the denoising modeling approach [11] to the proposed model, we first must prove the following lemma:

**Lemma 3.3.**  *$\tilde{\mu}_t(\mathbf{x}_t, \mathbf{x}_0, \boldsymbol{\xi})$  ( $t = 2, \dots, T$ ) in (27) can be expressed as follows:*

$$\tilde{\mu}_t(\mathbf{x}_t, \mathbf{x}_0, \boldsymbol{\xi}) = \frac{1}{\sqrt{\bar{\alpha}_t}}\mathbf{x}_t - \frac{1 - \alpha_t}{\sqrt{1 - \bar{\alpha}_t}\sqrt{\bar{\alpha}_t}}(\sigma_0\boldsymbol{\epsilon}_0 + \phi_t\boldsymbol{\xi}), \quad (30)$$

where  $\boldsymbol{\epsilon}_0 \sim \mathcal{N}(\boldsymbol{\epsilon}_0 | 0, I)$  and  $\phi_t$  ( $t = 2, \dots, T$ ) is given by (21).

*Proof.* See Appendix A.4. □

Instead of directly predicting  $\tilde{\mu}_t(\mathbf{x}_t, \mathbf{x}_0, \boldsymbol{\xi})$  with  $\mu_\theta(\mathbf{x}_t, t)$ , we adopt the form given in (8) for  $\mu_\theta(\mathbf{x}_t, t)$ , as proposed in [11]. In this formulation,  $\epsilon_\theta(\mathbf{x}_t, t)$  serves as the training target instead of  $\mu_\theta(\mathbf{x}_t, t)$ . Then, from Lemma 3.3, the KL divergence in  $\mathcal{L}_3$  can be transformed as follows:

$$D_{\text{KL}}(q(\mathbf{x}_{t-1}|\mathbf{x}_t, \mathbf{x}_0, \boldsymbol{\xi}) || p_\theta(\mathbf{x}_{t-1}|\mathbf{x}_t)) = \lambda_t \mathbb{E}_{\mathcal{N}(\boldsymbol{\epsilon}_0|0, I)} \left[ \|\sigma_0\boldsymbol{\epsilon}_0 + \phi_t\boldsymbol{\xi} - \epsilon_\theta(\mathbf{x}_t, t)\|^2 \right] + C_1, \quad (31)$$

where  $C_1$  is a constant independent of  $\theta$ .

### 3.2.4 Derivation of $\mathcal{L}_1$

From the definitions in (21) and (22), it follows that  $\phi_1 = \psi_1$ . Then, the expectation in  $\mathcal{L}_1$  takes the following form:

$$\mathbb{E}_{q(\mathbf{x}_1|\mathbf{x}_0,\boldsymbol{\xi})} [\log p_\theta(\mathbf{x}_0|\mathbf{x}_1)] = -\lambda_1 \mathbb{E}_{\mathcal{N}(\boldsymbol{\epsilon}_0|0,I)} \left[ \|\sigma_0 \boldsymbol{\epsilon}_0 + \phi_1 \boldsymbol{\xi} - \epsilon_\theta(\mathbf{x}_1, 1)\|^2 \right] + C_2, \quad (32)$$

where  $C_2$  is a constant independent of  $\theta$ . See Appendix A.5 for the detailed derivation of (32).

### 3.2.5 Derivation of the training loss function

From (31) and (32), the loss function for maximizing the variational lower bound in (23) with respect to  $\theta$  is given by  $\ell(\theta; \mathbf{x}_0)$  in (20), thus proving Theorem 3.1.

## 3.3 Comparison with existing models

Following [11], we define a simplified version of  $\ell(\theta; \mathbf{x}_0)$  by setting all  $\lambda_t$  in (20) to 1:

$$\ell_{\text{simple}}(\theta; \mathbf{x}_0) = \mathbb{E}_{q(\boldsymbol{\xi}), \mathcal{U}(t|1,T), \mathcal{N}(\boldsymbol{\epsilon}_0|0,I)} \left[ \left\| \sigma_0 \boldsymbol{\epsilon}_0 + \phi_t \boldsymbol{\xi} - \epsilon_\theta \left( \sqrt{\bar{\alpha}_t} \mathbf{x}_0 + \sqrt{1 - \bar{\alpha}_t} (\sigma_0 \boldsymbol{\epsilon}_0 + \psi_t \boldsymbol{\xi}), t \right) \right\|^2 \right] \quad (33)$$

**Comparison with offset noise model** The loss function of the offset noise model in (13) is similar to the loss function in (33) derived from the proposed model. However, the two differ in a key aspect. In the loss function of the proposed model,  $\boldsymbol{\xi} \sim q(\boldsymbol{\xi})$  is added to  $\boldsymbol{\epsilon}_0$  by weighting it with time-dependent coefficients  $\phi_t$  and  $\psi_t$ , whereas in the offset noise model,  $\boldsymbol{\epsilon}_c \sim q(\boldsymbol{\epsilon}_c)$  is added to  $\boldsymbol{\epsilon}_0$  with a constant coefficient of 1, independent of the time step. This difference is fundamental, as it arises from the fact that the proposed model is rigorously derived from the underlying probabilistic framework.

Besides having the above difference in the loss function, the offset noise model and the proposed model also differ in their reverse processes. As specified in (18), the proposed model initializes  $\mathbf{x}_T$  as Gaussian noise with mean  $\boldsymbol{\xi} \sim q(\boldsymbol{\xi})$  at the start of the reverse process. In contrast, the reverse process of the offset noise model typically employs a standard diffusion model, where  $\mathbf{x}_T$  is initialized as Gaussian noise with zero mean, as described in (4).

**Comparison with existing diffusion models** In the existing diffusion models described in subsection 2.1.1, the forward process diffuses the input  $\mathbf{x}_0$  into a Gaussian distribution with zero mean and variance  $I$ . In contrast, as shown in Proposition 3.2, the forward process in the proposed model diffuses  $\mathbf{x}_0$  into a Gaussian distribution with mean  $\boldsymbol{\xi}$  and variance  $\sigma_0^2 I$ . If we set  $q(\boldsymbol{\xi})$  to a delta function peaking at zero and  $\sigma_0 = 1$ , the proposed model becomes equivalent to the conventional diffusion model. Thus, it can be regarded as a generalization of the conventional diffusion model.

## 4 Method for constructing $\gamma_t$ in the proposed model

The values of  $\phi_t$  and  $\psi_t$  in the loss function of the proposed model are determined by  $\beta_t$  (or the derived values  $\alpha_t$  and  $\bar{\alpha}_t$ ) and  $\gamma_t$ , as shown in (21) and (22). Here, we will assume that  $\beta_t$  is a value used in the existing diffusion models and focus on the method of determining  $\gamma_t$ , which determines  $\phi_t$  and  $\psi_t$  in the proposed model.

### 4.1 Balanced- $\phi_t, \psi_t$ strategy

In the loss function (12) of the existing diffusion models, noise  $\boldsymbol{\epsilon}_0$  is added to  $\mathbf{x}_0$ , weighted by a time-dependent factor, to generate  $\mathbf{x}_t$ ; this added noise  $\boldsymbol{\epsilon}_0$  is then predicted by  $\epsilon_\theta$  using  $\mathbf{x}_t$ . Therefore, the noise added to  $\mathbf{x}_0$  and the target noise for the prediction are identical in (12). In the proposed model's loss function (20), the noise added to  $\mathbf{x}_0$  is  $\sigma_0 \boldsymbol{\epsilon}_0 + \psi_t \boldsymbol{\xi}$ , while the target noise for the prediction is  $\sigma_0 \boldsymbol{\epsilon}_0 + \phi_t \boldsymbol{\xi}$ . To preserve the

property of the loss function from existing diffusion models, it is natural to set  $\gamma_t$  such that  $\psi_t = \phi_t$ , ensuring that the added noise and the target noise are identical. We refer to this method of determining  $\gamma_t$  as the balanced- $\phi_t, \psi_t$  strategy. Its procedure is described below.

Assuming that  $\phi_t = \psi_t$  holds for  $t = 2, \dots, T$ , the following equation is obtained from (21) and (22):

$$\frac{\sqrt{\alpha_t}\sqrt{1-\bar{\alpha}_t}}{1-\alpha_t}\gamma_t = \frac{1}{\sqrt{1-\bar{\alpha}_t}}\sum_{i=1}^t\sqrt{\frac{\bar{\alpha}_t}{\bar{\alpha}_{i-1}}}\gamma_i$$

Rearranging this equation leads to the following expression for  $\gamma_t$ :

$$\gamma_t = \frac{(1-\alpha_t)\sqrt{\bar{\alpha}_{t-1}}}{\alpha_t(1-\bar{\alpha}_{t-1})}\sum_{i=1}^{t-1}\frac{\gamma_i}{\sqrt{\bar{\alpha}_{i-1}}} \quad (34)$$

Additionally, as discussed in subsection 3.2.4, the following relationship holds by definition:

$$\phi_1 = \psi_1 = \frac{\sqrt{\alpha_1}}{\sqrt{1-\alpha_1}}\gamma_1$$

Therefore, if  $\gamma_t$  ( $t = 2, \dots, T$ ) is determined recursively according to (34), the condition  $\phi_t = \psi_t$  ( $t = 1, \dots, T$ ) will be satisfied, and this condition does not depend on the value of  $\gamma_1$ .

In the balanced- $\phi_t, \psi_t$  strategy,  $\gamma_1$  is determined in a way that the condition  $\psi_T = 1$  in Proposition 3.2 holds: i.e., if we scale  $\gamma_1$  by a positive constant  $C(> 0)$ , then the recursively computed values  $\gamma_t$  ( $t \geq 2$ ) from (34), along with the derived  $\phi_t$  and  $\psi_t$  ( $t \geq 1$ ), are all scaled by  $C$ . Therefore, we set  $\hat{\gamma}_1 = 1$  and compute  $\hat{\gamma}_t$  ( $t \geq 2$ ) recursively with (34). Then, we use these values and (22) to calculate  $\hat{\psi}_T$ . Finally, we find that  $\gamma_t = \hat{\gamma}_t/\hat{\psi}_T$ . By leveraging the scaling property mentioned above, the condition  $\psi_T = 1$  is guaranteed to hold with  $\gamma_t$  obtained through this procedure.

The balanced- $\phi_t, \psi_t$  strategy is summarized as Algorithm 1.

---

**Algorithm 1** Balanced- $\phi_t, \psi_t$  strategy for constructing  $\gamma_t$

---

```

1:  $\hat{\gamma}_1 = 1$ 
2: for  $t = 2$  to  $T$  do
3:    $\hat{\gamma}_t = \frac{(1-\alpha_t)\sqrt{\bar{\alpha}_{t-1}}}{\alpha_t(1-\bar{\alpha}_{t-1})}\sum_{i=1}^{t-1}\frac{\hat{\gamma}_i}{\sqrt{\bar{\alpha}_{i-1}}}$ 
4: end for
5:  $\hat{\psi}_T = \frac{1}{\sqrt{1-\bar{\alpha}_T}}\sum_{i=1}^T\sqrt{\frac{\bar{\alpha}_T}{\bar{\alpha}_{i-1}}}\hat{\gamma}_i$ 
6: for  $t = 1$  to  $T$  do
7:    $\gamma_t = \hat{\gamma}_t/\hat{\psi}_T$ 
8: end for
9: return  $\gamma_t$  ( $t = 1, \dots, T$ )

```

---

## 4.2 $\tilde{\mu}_t$ under the balanced- $\phi_t, \psi_t$ strategy

When the balanced- $\phi_t, \psi_t$  strategy is used to determine  $\gamma_t$ , the following proposition holds:

**Proposition 4.1.** *Suppose that  $\gamma_t$  in the proposed model is determined using the balanced- $\phi_t, \psi_t$  strategy and  $\sigma_0 = 1$ . Then,  $q(\mathbf{x}_{t-1}|\mathbf{x}_t, \mathbf{x}_0, \boldsymbol{\xi})$  in (26) coincides with  $q(\mathbf{x}_{t-1}|\mathbf{x}_t, \mathbf{x}_0)$  in standard diffusion models [11].*

*Proof.* As shown in Appendix A.4, the relationship  $\phi_t = \psi_t - \frac{\sqrt{1-\bar{\alpha}_t}\sqrt{\alpha_t}}{1-\alpha_t}\nu_t$  ( $t = 2, \dots, T$ ) holds. For  $\gamma_t$  determined by the balanced- $\phi_t, \psi_t$  strategy,  $\phi_t = \psi_t$ , which implies  $\nu_t = 0$  ( $t = 2, \dots, T$ ). In this case, from (27),  $\tilde{\mu}_t(\mathbf{x}_t, \mathbf{x}_0, \boldsymbol{\xi})$  in the proposed model is independent of  $\boldsymbol{\xi}$ . Consequently,  $q(\mathbf{x}_{t-1}|\mathbf{x}_t, \mathbf{x}_0, \boldsymbol{\xi})$  in the proposed model coincides with  $q(\mathbf{x}_{t-1}|\mathbf{x}_t, \mathbf{x}_0)$  in standard diffusion models [11], under the assumption that  $\sigma_0 = 1$ .  $\square$

### 4.3 Example calculation of $\gamma_t$

Here, we present a concrete example of determining  $\gamma_t$ ,  $\psi_t$ , and  $\phi_t$  by using the balanced- $\phi_t, \psi_t$  strategy. In particular, it uses the  $\beta_t$  values of Stable Diffusion 1.5 [26], with  $T$  set to 1000. Figure 1 illustrates  $\gamma_t$  computed using the balanced- $\phi_t, \psi_t$  strategy, along with the corresponding  $\psi_t$  and  $\phi_t$  determined by  $\gamma_t$  for these values of  $\beta_t$ . This figure indicates that the ranges of  $\beta_t$  and  $\gamma_t$  are similar; however,  $\gamma_t$  shows a steeper increase at larger time steps compared with  $\beta_t$ . Moreover,  $\psi_t$  and  $\phi_t$  are identical across all time steps and converge to 1 at  $T = 1000$ .

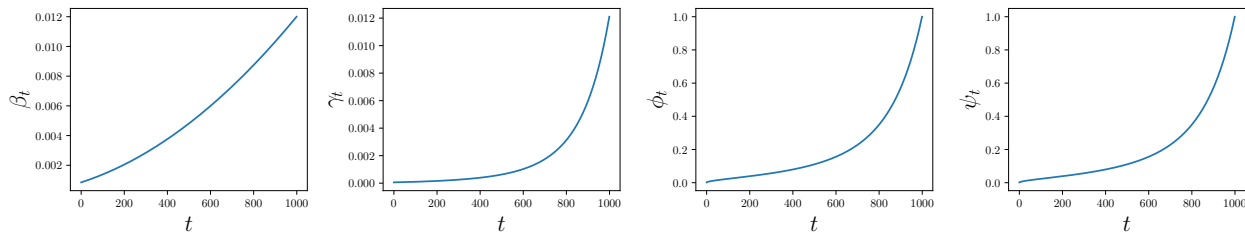


Figure 1: From left to right, the figure illustrates  $\beta_t$  used in Stable Diffusion 1.5, along with the corresponding  $\gamma_t$ ,  $\phi_t$ , and  $\psi_t$  computed using the balanced- $\phi_t, \psi_t$  strategy (the horizontal axis represents time  $t$ ).

As shown in Figure 1, both  $\phi_t$  and  $\psi_t$  tend to gradually increase with time  $t$ . With regard to the loss function of the proposed model (20), this behavior implies that the coefficient associated with the additional noise  $\xi$  increases as time  $t$  progresses. Consequently, the closer  $\mathbf{x}_t$  is to  $\mathbf{x}_0$ , the smaller is the coefficient applied to  $\xi$  when it is added to  $\epsilon_0$ . It is noteworthy that such behavior of  $\phi_t$  and  $\psi_t$  emerges naturally from the assumption of  $\phi_t = \psi_t$  in the balanced- $\phi_t, \psi_t$  strategy.

## 5 Extension to $v$ -prediction modeling

The proposed model is theoretically grounded in a well-defined probabilistic framework and supports integration with other diffusion model methods. Such theoretically grounded integrations would be difficult to achieve with the offset noise model.

As an example, we extend the proposed model to  $v$ -prediction [27]. In  $v$ -prediction,  $\mu_\theta$  is reparameterized using  $v_\theta$ , which is referred to as velocity, instead of  $\epsilon_\theta$ . While reparameterization with  $\epsilon_\theta$  requires  $\alpha_t \neq 0$  in accordance with its definition in (8), reparameterization with  $v_\theta$  eliminates this restriction. This property has been exploited in methods such as the one in [19]. Moreover,  $v$ -prediction has been employed in recent text-conditional image generation models, including Stable Diffusion 2 [26, 30].

### 5.1 Training loss function in $v$ -prediction modeling

The following proposition defines the training loss function for the proposed model under  $v$ -prediction modeling:

**Proposition 5.1** (Training loss function for  $v$ -prediction). *Suppose the forward and reverse processes in (14)–(19) and  $\gamma_t$  ( $t = 1, \dots, T$ ) are determined by the balanced- $\phi_t, \psi_t$  strategy. Then, the loss function that maximizes the evidence lower bound in (23) under  $v$ -prediction modeling is given by*

$$\ell^v(\theta; \mathbf{x}_0) = \mathbb{E}_{q(\xi), \mathcal{U}(t|1, T), \mathcal{N}(\epsilon_0|0, I)} \left[ \lambda_t^v \left\| \sqrt{\bar{\alpha}_t} (\sigma_0 \epsilon_0 + \psi_t \xi) - \sqrt{1 - \bar{\alpha}_t} \mathbf{x}_0 - v_\theta(\mathbf{x}_t, t) \right\|^2 \right],$$

where  $\lambda_t^v$  is given by

$$\lambda_t^v = \frac{\bar{\alpha}_{t-1}(1 - \alpha_t)^2}{2\sigma_t^2(1 - \bar{\alpha}_t)},$$

and  $\psi_t$  and  $\mathbf{x}_t$  are given by (22) and (24), respectively.

*Proof.* See Appendix A.6. □

## 6 Related work

**Offset noise and its variants** An online technical report by Guttenberg [9] was among the first to point out that Stable Diffusion, a widely used text-conditional image generation diffusion model, struggles to generate images with extreme average brightness. In that report, Guttenberg analyzed the underlying causes of these brightness-related issues and introduced offset noise as a potential solution, as described in subsection 2.2. Additionally, an extended variant of offset noise, referred to as pyramid noise, was proposed in [33]. However, both approaches involve making modifications to the final loss function derived from the diffusion model, but leave it unclear how their adjustments correspond to changes in the probabilistic framework underlying the diffusion process.

**Other approaches to mitigating brightness issues** Lin et al. [19] analyzed the scheduling of  $\beta_t$  in diffusion models and proposed a method to adjust it so that the signal-to-noise ratio (SNR) reaches zero at the final time step  $T$  of the forward process. They experimentally demonstrated that this adjustment effectively mitigates brightness issues in Stable Diffusion. However, the  $\beta$  values corrected by their method impose a limitation in which the  $\epsilon$ -prediction framework becomes inapplicable, prompting Lin et al. to recommend adopting the  $v$ -prediction framework as an alternative to overcome this problem.

Hu et al. [12] proposed a method that trains an additional model to correct the initial noise in the reverse process of a pre-trained diffusion model. They experimentally demonstrated that incorporating the corrected initial noise into the reverse process effectively mitigates brightness issues. While their approach has the advantage of leveraging existing pre-trained models, it may require training of additional auxiliary models when constructing new diffusion models, potentially leading to inefficiencies.

**Diffusion into non-Gaussian distributions** As alternatives to continuous-time diffusion models that diffuse inputs to a standard Gaussian distribution, Schrödinger bridge approaches [4, 20, 2] and flow-matching-based approaches [21, 31] have been explored as ways of generating conditional probabilities. Unlike diffusion models, these approaches learn a path or a vector field between the data distribution and another distribution, which does not necessarily need to be a standard Gaussian. There may be a potential connection between the proposed model and approaches based on Schrödinger bridges or flow matching, as both involve diffusing the data distribution into a target distribution distinct from the standard normal. However, we will leave such an investigation for future work.

## 7 Experiments

In this section, we report the results of experiments comparing the proposed model with existing methods, focusing on the challenge diffusion models face in generating images with extreme brightness levels. Regarding this issue, prior studies [9, 19, 12] have evaluated text-conditioned image generation models by examining scenarios such as whether a truly black image can be generated under text conditions like "Solid black background." However, their evaluations were qualitative, focusing on a specific subset of the learned distribution, and did not provide a quantitative assessment of overall distribution modeling performance.

To the best of the authors' knowledge, no image benchmark dataset currently exists that includes images with extreme brightness levels while maintaining a controlled distribution. To fill this gap, we generated synthetic data simulating a scenario where the brightness distribution is uniform. Using this artificial dataset, we performed quantitative evaluations of the proposed method. The experiments revealed that, particularly in high-dimensional settings, the brightness distribution of the data generated by existing diffusion models was not uniform, even when they were trained on data with a uniform brightness distribution. In particular, images with low or high brightness levels were relatively less likely to be generated. These results indicated

that the synthetic data generated in this study could expose the challenge faced by diffusion models in generating images with extreme brightness levels.

Below, we describe the procedure for generating the synthetic data used in the experiments and its statistical properties. Subsequently, we detail the experimental setup and present the results.

## 7.1 Dataset

The generated dataset is referred to as the Cylinder dataset. It consists of data points  $\mathbf{x}_0 \in \mathbb{R}^n$  that are, as the name suggests, distributed in a cylindrical shape within an  $n$ -dimensional space. The center of the top face of the cylinder is defined as  $\mathbf{x}_{\text{top}} := k\mathbf{1}_n$ , and the center of the bottom face is defined as  $\mathbf{x}_{\text{bottom}} := -\mathbf{x}_{\text{top}}$ , where  $k (> 0)$  is a scalar and  $\mathbf{1}_n$  is an  $n$ -dimensional vector with all elements equal to 1. Additionally, the radius of the cylinder is defined as  $r\|\mathbf{1}_n\|$  ( $r > 0$ ).  $\mathbf{x}_0$  is generated according to the following equation:

$$\mathbf{x}_0 = u_h\mathbf{x}_{\text{top}} + u_r\mathbf{x}_{\text{ortho}}, \quad (35)$$

where  $u_h$  and  $u_r$  are random scalar variables given by  $u_h \sim \mathcal{U}_c(-1, 1)$  and  $u_r \sim \mathcal{U}_c(0, r)$ , respectively. Here,  $\mathcal{U}_c(a, b)$  denotes a uniform distribution over  $[a, b]$ . Additionally,  $\mathbf{x}_{\text{ortho}}$  is a random unit vector in the subspace  $\mathbf{1}_n^\perp$ , which is orthogonal to  $\mathbf{1}_n$ . For reference, the python code used to create the Cylinder dataset is provided in Appendix B.

### 7.1.1 Brightness distribution of the Cylinder dataset

Consider a grayscale image  $\mathbf{x}^{\text{im}}$  with  $n$  pixels. For convenience, we will assume that each element of  $\mathbf{x}^{\text{im}}$  is normalized to fall within the range  $[-k, k]$ . Each element of  $\mathbf{x}^{\text{im}}$  represents the brightness of a pixel. The average brightness of  $\mathbf{x}^{\text{im}}$  is defined as follows:

$$L_{\text{avg}}(\mathbf{x}^{\text{im}}) := \frac{1}{n}\mathbf{x}^{\text{im}} \cdot \mathbf{1}_n$$

The image with the lowest average brightness is one where all elements are  $-k$  (a completely black image), while the image with the highest average brightness is one where all elements are  $k$  (a completely white image).

If the data points  $\mathbf{x}_0$  in the Cylinder dataset are regarded as pseudo grayscale images,<sup>5</sup> then, by definition,  $\mathbf{x}_{\text{bottom}}$  and  $\mathbf{x}_{\text{top}}$  correspond to a completely black image and a completely white image, respectively. From the definition in (35),  $\mathbf{x}_0$  can be interpreted as the sum of two images,  $u_h\mathbf{x}_{\text{top}}$  and  $u_r\mathbf{x}_{\text{ortho}}$ , whose average brightness can be computed as follows:

$$\begin{aligned} L_{\text{avg}}(u_h\mathbf{x}_{\text{top}}) &= \frac{1}{n}u_h\mathbf{x}_{\text{top}} \cdot \mathbf{1}_n = \frac{u_h k \mathbf{1}_n \cdot \mathbf{1}_n}{n} = u_h k \sim \mathcal{U}_c(-k, k), \\ L_{\text{avg}}(u_r\mathbf{x}_{\text{ortho}}) &= \frac{1}{n}u_r\mathbf{x}_{\text{ortho}} \cdot \mathbf{1}_n = 0, \end{aligned}$$

where we have used the fact that  $\mathbf{x}_{\text{ortho}} \in \mathbf{1}_n^\perp$  implies  $\mathbf{x}_{\text{ortho}} \cdot \mathbf{1}_n = 0$ . The average brightness of  $\mathbf{x}_0$  is then

$$L_{\text{avg}}(\mathbf{x}_0) = \frac{1}{n}(u_h\mathbf{x}_{\text{top}} + u_r\mathbf{v}) \cdot \mathbf{1}_n = L_{\text{avg}}(u_h\mathbf{x}_{\text{top}}) + L_{\text{avg}}(u_r\mathbf{v}) = u_h k \sim \mathcal{U}_c(-k, k) \quad (36)$$

Therefore, if  $\mathbf{x}_0$  in the Cylinder dataset is interpreted as a pseudo grayscale image, the average brightness of  $\mathbf{x}_0$  is uniformly distributed within the range  $[-k, k]$ .

### 7.1.2 Experimental setup for the Cylinder dataset

The dimensionality  $n$  was varied as follows:  $n = 2, 10, 50, 100, 200$ . For each value of  $n$ , training and test Cylinder datasets, each containing 5000 samples, were generated by following the procedure described in

<sup>5</sup>Strictly speaking,  $\mathbf{x}_0$  cannot be considered a true grayscale image because it does not strictly lie within  $[-k, k]^n$ .

Section 7.1. The parameters  $k$  and  $r$  were set to  $k = 2$  and  $r = 0.5$ , respectively. These values were selected to ensure that the standard deviation of each component in the generated Cylinder dataset was close to 1.<sup>6</sup> An example of a Cylinder dataset with  $n = 2$  is shown in the rightmost column of Figure 2.

## 7.2 Compared models

We used the following models as comparisons:

- *Base model*: This model employs the training loss function  $\hat{\ell}_{\text{simple}}$  from (12), which corresponds to the one used in the DDPM model [11].
- *Offset noise model*: This model adopts the loss function  $\hat{\ell}_{\text{offset}}$  in (13). Since  $\mathbf{x}_0$  in the Cylinder dataset represents grayscale images (single-channel), we define  $q(\boldsymbol{\epsilon}_c) = \mathcal{N}(\boldsymbol{\epsilon}_c \mid 0, \sigma_c^2 \mathbf{1}_{n \times n})$ , where  $\mathbf{1}_{n \times n}$  is an  $n \times n$  matrix with all elements equal to 1.
- *Zero-SNR model*: This model modifies  $\beta_t$  in the Base model by using the method proposed in [19].
- *Proposed model*: This model employs the training loss function  $\ell_{\text{simple}}$  defined in (33), where  $\gamma_t$  is determined by the balanced- $\phi_t, \psi_t$  strategy and  $\sigma_0 = 1$ . In the proposed model,  $q(\boldsymbol{\xi})$  is set to be identical to  $q(\boldsymbol{\epsilon}_c)$  in the Offset noise model. Thus, in our experiments, the only difference between the loss functions of the proposed model and the offset noise model was the proposed one’s inclusion of the two coefficients,  $\phi_t$  and  $\psi_t$ .

Additionally, for each of the above models, we employed versions that utilize  $v$ -prediction [27]. It should be noted that although there is no theoretical guarantee that offset noise will work within the  $v$ -prediction framework, as was discussed in section 5, it is practically feasible to incorporate offset noise into the  $v$ -prediction model by replacing  $\boldsymbol{\epsilon}_0$  in the loss function with  $\boldsymbol{\epsilon}_0 + \boldsymbol{\epsilon}_c$ , analogously to its application in  $\epsilon$ -prediction modeling. Furthermore, for the Zero-SNR model, only the version utilizing  $v$ -prediction was employed, as its formulation prohibits the use of  $\epsilon$ -prediction modeling.

For the Offset Noise model, the hyperparameter  $\sigma_c^2$  was varied across the values 0.01, 0.05, 0.1, 0.5, and 1.0, with training and evaluation conducted for each setting. Similarly, for the proposed model,  $\sigma_c^2$  was varied across 0.1, 0.5, and 1.0, and training and evaluation were performed for each configuration.

## 7.3 Training and sampling settings

**Settings for  $\epsilon_\theta$  and  $\beta_t$  in the diffusion model** As the model for  $\epsilon_\theta$  (or  $v_\theta$  in the case of  $v$ -prediction), we used a multilayer perceptron (MLP) that had been extended to incorporate the time step  $t$  as part of its input. The MLP architecture consisted of five hidden layers, each employing the GELU activation function [10], with the number of neurons set to 256, 512, 1024, 512, and 256 in each layer, respectively. The maximum diffusion time was set to  $T = 200$ , and  $\beta_t$  was determined using a log-linear schedule [24].<sup>7</sup>

**Optimizer settings** We used the Adam optimizer [16] for training, setting the learning rate to 0.001. The mini-batch size was fixed at 1024, and training was carried out for 200,000 steps. For some models, including Base, the loss function occasionally diverged during training depending on the random seed. To mitigate this issue and stabilize the training process, gradient clipping [23] was applied, limiting the maximum gradient norm at 1 during training.

<sup>6</sup>The actual standard deviation of each component in the generated Cylinder dataset was approximately 1.2, regardless of the dimensionality  $n$ . Furthermore, due to the symmetry of the Cylinder dataset around the origin, the mean of each component was 0.

<sup>7</sup>We utilized the `TimeInputMLP` and `ScheduleLogLinear` modules available at <https://github.com/yuanchenyang/smalldiffusion> (accessed 2024/10/4), for the MLP model and beta scheduling, respectively. In `ScheduleLogLinear`, we set `sigma_min` to 0.01 and `sigma_max` to 10.

**Settings for the reverse process** When generating new data through the reverse process using the trained models, we set the maximum time step to  $T = 200$ . To prevent the generated data from diverging, clipping was applied at each step of the reverse process to ensure that the data remained within the range  $[-10, 10]^n$ .<sup>8</sup>

## 7.4 Evaluation metrics

We had each trained model generate 5000 new data samples through the reverse process and evaluated each one by measuring the distance between the generated data distribution and the test dataset distribution. Two metrics were used to quantify this distance: the 1-Wasserstein distance [32] and the maximum mean discrepancy [7], hereafter referred to as 1WD and MMD, respectively. For MMD, a Gaussian kernel was used with its bandwidth parameter set to  $\sqrt{n}$ . Six pairs of training and test datasets were created by varying the random seed, and each model was trained and evaluated on all six pairs. Note that model initialization and other training factors were also randomized based on the seed.

## 7.5 Generation examples

Figure 2 illustrates examples of data generated through the reverse process using the trained models with  $n = 2$ . The upper and lower rows in the figure depict the data distributions at each time step during the reverse process for the Base and Proposed model (with  $\sigma_c^2 = 1.0$ ), respectively. The rightmost column represents the test dataset. It can be seen that for  $n = 2$ , both models generated data distributions at  $t = 0$  that are very close to the test dataset distribution. The Proposed model’s distribution at time  $T$  is a Gaussian distribution with a mean of  $\xi \sim \mathcal{N}(\xi|0, \sigma_c^2 \mathbf{1}_{n \times n})$ , as described in subsection 7.2, whereas the Base model has a Gaussian distribution with a mean of 0 at time  $T$  ( $T = 200$  in this case). Consequently, at  $T = 200$ , the Proposed model’s distribution is more spread out in the diagonal directions compared with that of the Base model.

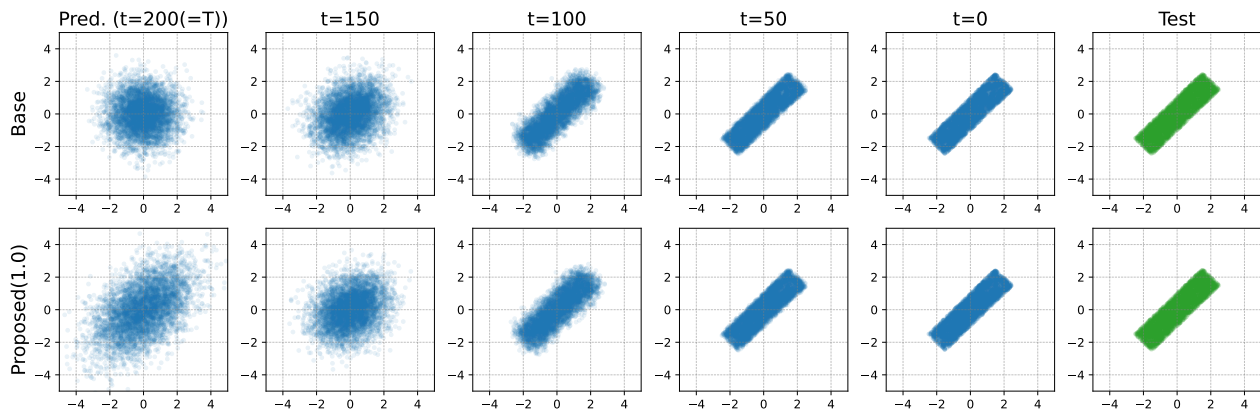


Figure 2: Distribution of generated data with  $n = 2$  at each time step during the reverse process. The rightmost column represents the test data. The top row shows the results of the Base model, while the bottom row illustrates those of the Proposed model ( $\sigma_c^2 = 1.0$ ).

## 7.6 Evaluation results

We had each model generate new data points through the reverse process every 5000 steps during training and measured their distance to the test dataset by using 1WD and MMD. The results in Figure 3 are for the  $\epsilon$ -prediction models. The solid lines (or dashed and dotted lines, as applicable) in the figure represent the medians over six trials, while the error bars indicate the 10th to 90th percentiles. For the Offset noise

<sup>8</sup>Such clipping is frequently applied in diffusion models for images. In this study, we used a relatively large threshold of 10, compared with the distribution of the Cylinder dataset, which is roughly within the range  $[-3, 3]^n$ . This choice allows any divergence that occurs to be partially reflected in the evaluation results, while avoiding numerical instabilities.

model, the evaluation results for  $\sigma_c^2 = 1.0$  were consistently worse than those for  $\sigma_c^2 = 0.5$ . Therefore, the results for  $\sigma_c^2 = 1.0$  are omitted from the graph.

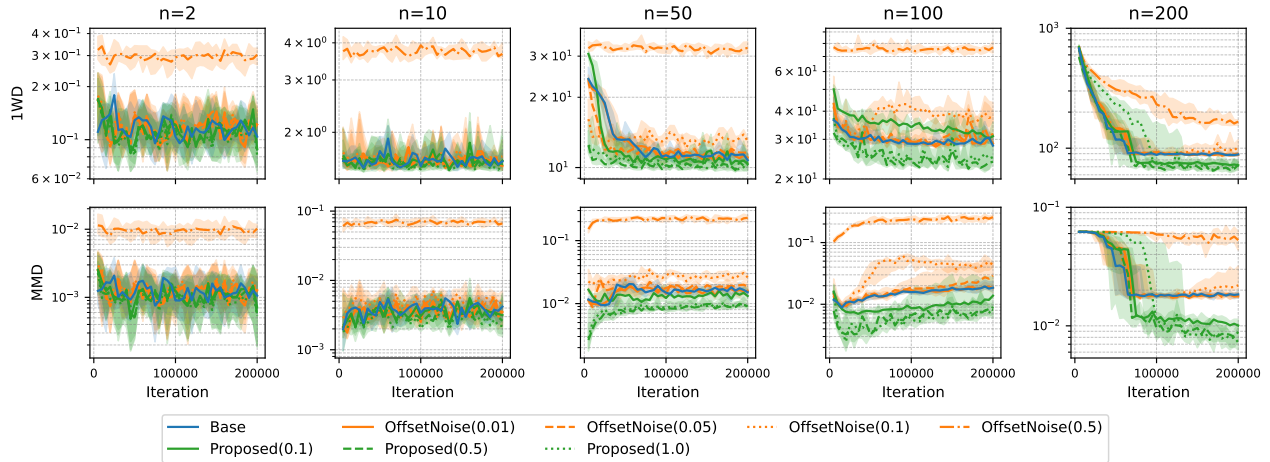


Figure 3: Evaluation results of 1WD (top row) and MMD (bottom row) during training.

From Figure 3, it can be observed that for  $n \leq 10$ , all models except the Offset noise model ( $\sigma_c^2 = 0.5$ ) have similar evaluation metrics. As the dimensionality  $n$  increases, the Proposed model outperforms the other models by achieving smaller 1WD and MMD values. These results suggest that the Proposed model can more accurately approximate the distribution of the Cylinder dataset, characterized by a uniform brightness distribution, particularly in higher-dimensional cases.

For the Cylinder dataset used in this study, applying offset noise did not yield any significant effects, and the reasons for this outcome remain unclear. To the best of the authors' knowledge, previous studies have not conducted any quantitative evaluations of offset noise comparable to those performed in this work. Therefore, it is difficult to ascertain whether the results observed here are anomalous or representative.

### 7.6.1 Comparison of average brightness distributions

In addition to the quantitative evaluations using 1WD and MMD described above, we compared the test dataset and the generated data by examining the distribution of the average brightnesses  $L_{\text{avg}}(\mathbf{x}_0)$ . As shown in (36), the average brightness  $L_{\text{avg}}(\mathbf{x}_0)$  in the Cylinder dataset follows a uniform distribution  $\mathcal{U}_c(-k, k)$ , where  $k = 2$  in this experiment.

The results are shown in Figure 4. In the figure, the results for the Base model, the Offset noise model ( $\sigma_c^2 = 0.1$ ), and the Proposed model ( $\sigma_c^2 = 1.0$ ) are presented in the top, middle, and bottom rows, respectively, for each  $n$ . The models used were those obtained after the final training step (200,000) for each setting. Similar to Figure 3, when  $n$  is relatively small ( $n \leq 10$ ), the distribution of  $L_{\text{avg}}(\mathbf{x}_0)$  in the generated data closely matches that of the test dataset for all models. As the dimension  $n$  increases, the  $L_{\text{avg}}(\mathbf{x}_0)$  distribution of the data generated by the Base and Offset noise models deviates from that of the test dataset. Specifically, in the case of the Base model with  $n = 200$ , the data near  $L_{\text{avg}}(\mathbf{x}_0) \approx -2$  are less likely to be generated. This highlights the difficulty diffusion models have in generating low-brightness images. In contrast, the proposed model consistently generates data whose  $L_{\text{avg}}(\mathbf{x}_0)$  distribution remains close to that of the test dataset, even as the dimension  $n$  increases.

### 7.6.2 Discussion on the effect of data dimensionality

One possible reason that the Base model generated images with extreme average brightness values less frequently as the dimension  $n$  increases is as follows (note that this is an alternative perspective to the

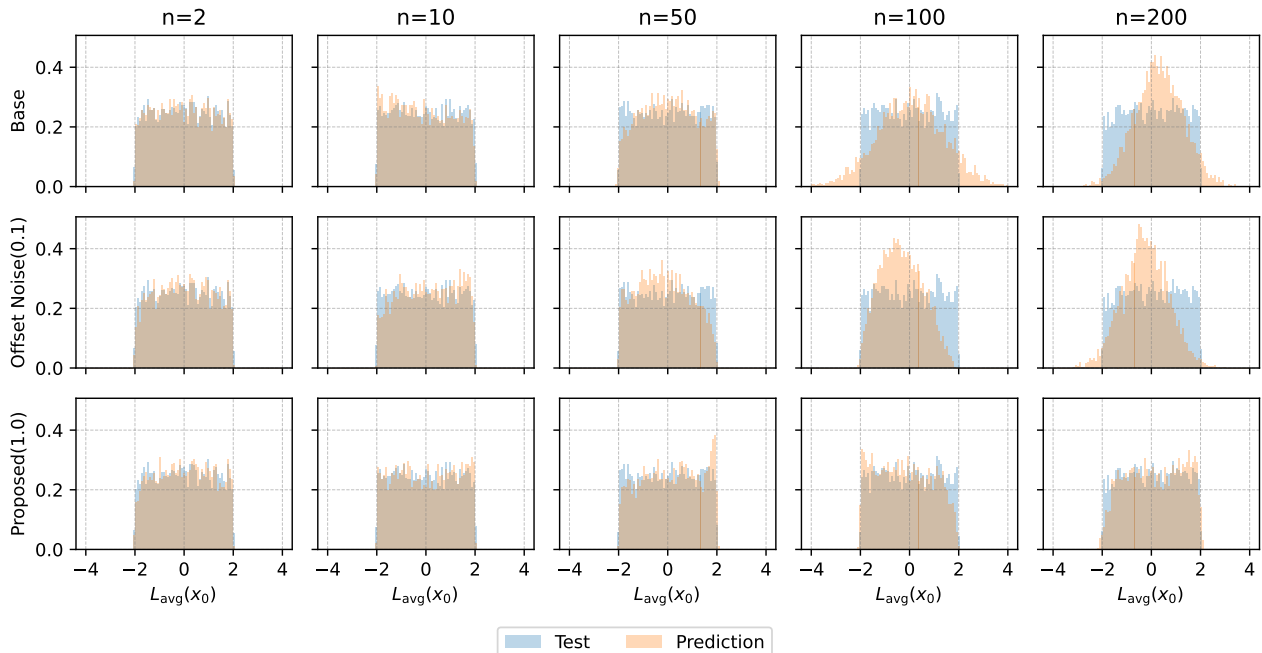


Figure 4: Comparison of distributions of average brightnesses  $L_{\text{avg}}(\mathbf{x}_0)$  between the test data and the generated data.

image frequency viewpoint discussed in subsection 2.2). In existing diffusion models, the average brightness  $L_{\text{avg}}(\mathbf{x}_T)$  of the diffused data  $\mathbf{x}_T$  is defined as the mean of  $n$  independent one-dimensional standard normal distributions. Consequently, the variance of  $L_{\text{avg}}(\mathbf{x}_T)$  is  $\frac{1}{n}$ , which diminishes and approaches 0 as the dimension  $n$  increases. This concentration around 0 makes it increasingly challenging to generate  $\mathbf{x}_0$  through the reverse process starting from  $\mathbf{x}_T$ , especially in the Cylinder dataset where  $L_{\text{avg}}(\mathbf{x}_0)$  is uniformly distributed regardless of  $n$ .

In contrast, by appropriately selecting  $q(\xi)$ , the proposed model prevents the variance of  $L_{\text{avg}}(\mathbf{x}_T)$  from converging to zero. This distinction is considered as a key factor underlying the performance difference between the Base model and the Proposed one, as illustrated in Figure 4.

### 7.6.3 Training with data scaling

It is known that scaling the dataset used for training diffusion models can affect the learning outcome [26]. Instead of using the original training data  $\mathbf{x}_0$  directly, the diffusion model is trained on  $\mathbf{x}_0/\rho$ , where  $\rho (> 0)$  represents the scaling parameter. After training, the final output is obtained by scaling the data generated by the trained diffusion model with the factor  $\rho$ .

The results of training the Base model with the data scaling applied to the Cylinder dataset are summarized in Appendix C.1. As can be seen, applying data scaling to the Cylinder dataset ( $n = 200$ ) does not significantly affect the distribution of  $L_{\text{avg}}(\mathbf{x}_0)$  in the generated outputs. This finding suggests that merely applying data scaling in the Base model does not overcome the challenge of generating data with extreme average brightness.

## 7.7 Evaluation results of $v$ -prediction models

Each model was trained within the  $v$ -prediction framework, and evaluations based on 1WD and MMD were conducted every 5000 training steps. The results are shown in Figure 5.

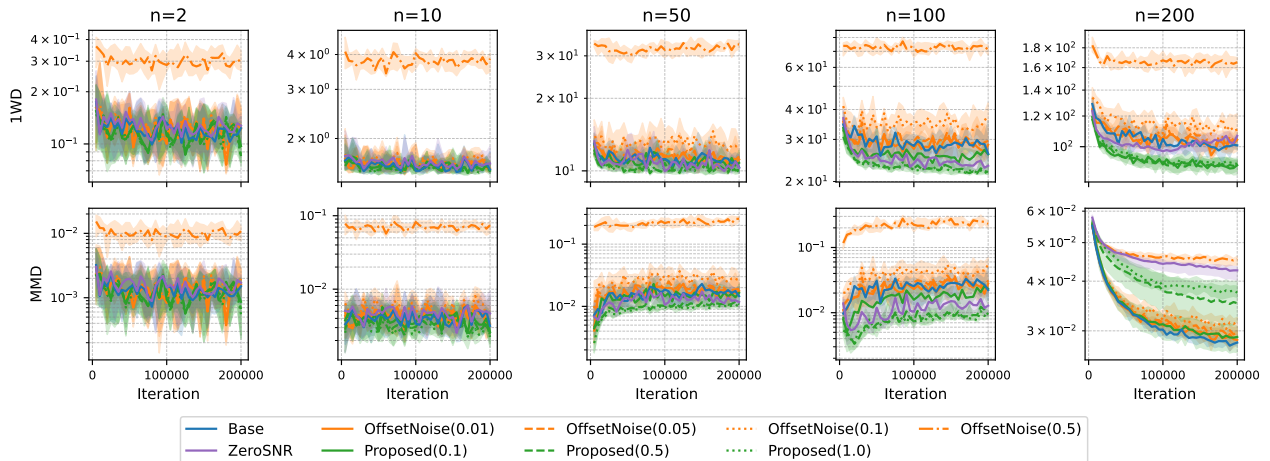


Figure 5: Evaluation results of 1WD (top) and MMD (bottom) during training within the  $v$ -prediction framework.

Similar to Figure 3, all models, except for the Offset noise model ( $\sigma_c^2 = 0.5$ ), achieved comparable evaluation scores for  $n \leq 10$ . As the dimensionality  $n$  increased, differences between the models became evident. Notably, for  $n = 200$ , the Proposed model achieved a lower 1WD compared with the other models. However, when the evaluation was conducted with MMD, the Proposed model underperformed the Base model for  $n = 200$ . Upon further investigation, we found that when generating data using the Proposed model with  $n = 200$ , some data points diverged during the reverse process, eventually deviating from the distribution of the test dataset. These outlier points comprised approximately 10 out of the 5000 generated data points, accounting for about 0.2% of the total. Due to MMD’s high sensitivity to outliers, these points likely contributed to the deterioration of the MMD score. In contrast, 1WD is less sensitive than MMD to outliers. Therefore, the results in Figure 5, showing higher MMD and lower 1WD for the Proposed model, suggest that although some outliers are present, the overall distribution of the generated data, excluding these outliers, more closely aligns with the distribution of the test dataset.

The comparison of the distributions of  $L_{\text{avg}}(\mathbf{x}_0)$  between the data generated by each  $v$ -prediction model and the test dataset is summarized in Appendix C.1.1. Similar to Figure 4, the Base model shows a divergence in the  $L_{\text{avg}}(\mathbf{x}_0)$  distribution of the generated data from that of the test dataset as the dimensionality  $n$  increases. In contrast, the Proposed model achieves a distribution that remains closer to the test dataset even at  $n = 200$ . These results suggest that even when  $v$ -prediction is employed, the Base model encounters difficulties in generating data with extreme brightness. The Proposed model effectively alleviates this issue within the  $v$ -prediction framework.

## 8 Conclusion and Future Work

We proposed a novel model for discrete-time diffusion processes that introduces an additional random variable  $\boldsymbol{\xi} \sim q(\boldsymbol{\xi})$ . We derived an evidence lower bound on the log-likelihood for the proposed model and demonstrated that the resulting loss function closely resembles the loss function obtained when offset noise is applied to conventional diffusion models. This study provides a theoretical interpretation for offset noise, which has been empirically effective, but has lacked a rigorous theoretical foundation. Moreover, it offers a new perspective on offset noise, broadening its applicability in practical scenarios.

As to future research directions, several possibilities can be explored. In this study, the distribution  $q(\boldsymbol{\xi})$  was predefined; however, an extension that allows  $q(\boldsymbol{\xi})$  to be estimated in a data-driven manner is worth investigating. Furthermore, while this work focused on the case where  $\mathbf{x}_0$  and  $\boldsymbol{\xi}$  are not paired with each

other, future studies could address scenarios where they are provided in a paired format. For example, one could consider a scenario where  $\mathbf{x}_0$  represents a high-resolution image and  $\boldsymbol{\xi}$  is its corresponding low-resolution counterpart. In such cases, the proposed model could potentially enable super-resolution tasks for  $\boldsymbol{\xi}$ .

## A Proofs and formula derivations

### A.1 Derivation of (23)

$$\begin{aligned}
& \log p_\theta(\mathbf{x}_0) \\
& \geq \mathbb{E}_{q(\mathbf{x}_{1:T}, \boldsymbol{\xi} | \mathbf{x}_0)} \left[ \log \frac{p_\theta(\mathbf{x}_{0:T}, \boldsymbol{\xi})}{q(\mathbf{x}_{1:T}, \boldsymbol{\xi} | \mathbf{x}_0)} \right] \\
& = \mathbb{E}_{q(\mathbf{x}_{1:T}, \boldsymbol{\xi} | \mathbf{x}_0)} \left[ \log \frac{p(\boldsymbol{\xi}) p(\mathbf{x}_T | \boldsymbol{\xi}) \prod_{t=1}^T p_\theta(\mathbf{x}_{t-1} | \mathbf{x}_t)}{q(\boldsymbol{\xi}) \prod_{t=1}^T q(\mathbf{x}_t | \mathbf{x}_{t-1}, \boldsymbol{\xi})} \right] \\
& = \mathbb{E}_{q(\mathbf{x}_{1:T}, \boldsymbol{\xi} | \mathbf{x}_0)} \left[ \log \frac{p(\mathbf{x}_T | \boldsymbol{\xi}) p_\theta(\mathbf{x}_0 | \mathbf{x}_1) \prod_{t=2}^T p_\theta(\mathbf{x}_{t-1} | \mathbf{x}_t)}{q(\mathbf{x}_1 | \mathbf{x}_0, \boldsymbol{\xi}) \prod_{t=2}^T q(\mathbf{x}_t | \mathbf{x}_{t-1}, \boldsymbol{\xi})} \right] \\
& = \mathbb{E}_{q(\mathbf{x}_{1:T}, \boldsymbol{\xi} | \mathbf{x}_0)} \left[ \log \frac{p(\mathbf{x}_T | \boldsymbol{\xi}) p_\theta(\mathbf{x}_0 | \mathbf{x}_1) \prod_{t=2}^T p_\theta(\mathbf{x}_{t-1} | \mathbf{x}_t)}{q(\mathbf{x}_1 | \mathbf{x}_0, \boldsymbol{\xi}) \prod_{t=2}^T q(\mathbf{x}_t | \mathbf{x}_{t-1}, \mathbf{x}_0, \boldsymbol{\xi})} \right] \\
& = \mathbb{E}_{q(\mathbf{x}_{1:T}, \boldsymbol{\xi} | \mathbf{x}_0)} \left[ \log \frac{p(\mathbf{x}_T | \boldsymbol{\xi}) p_\theta(\mathbf{x}_0 | \mathbf{x}_1)}{q(\mathbf{x}_1 | \mathbf{x}_0, \boldsymbol{\xi})} + \log \prod_{t=2}^T \frac{p_\theta(\mathbf{x}_{t-1} | \mathbf{x}_t)}{q(\mathbf{x}_t | \mathbf{x}_{t-1}, \mathbf{x}_0, \boldsymbol{\xi})} \right] \\
& = \mathbb{E}_{q(\mathbf{x}_{1:T}, \boldsymbol{\xi} | \mathbf{x}_0)} \left[ \log \frac{p(\mathbf{x}_T | \boldsymbol{\xi}) p_\theta(\mathbf{x}_0 | \mathbf{x}_1)}{q(\mathbf{x}_1 | \mathbf{x}_0, \boldsymbol{\xi})} + \log \prod_{t=2}^T \frac{p_\theta(\mathbf{x}_{t-1} | \mathbf{x}_t)}{\frac{q(\mathbf{x}_{t-1} | \mathbf{x}_t, \mathbf{x}_0, \boldsymbol{\xi}) q(\mathbf{x}_t | \mathbf{x}_0, \boldsymbol{\xi})}{q(\mathbf{x}_{t-1} | \mathbf{x}_0, \boldsymbol{\xi})}} \right] \\
& = \mathbb{E}_{q(\mathbf{x}_{1:T}, \boldsymbol{\xi} | \mathbf{x}_0)} \left[ \log \frac{p(\mathbf{x}_T | \boldsymbol{\xi}) p_\theta(\mathbf{x}_0 | \mathbf{x}_1)}{q(\mathbf{x}_1 | \mathbf{x}_0, \boldsymbol{\xi})} + \log \frac{q(\mathbf{x}_1 | \mathbf{x}_0, \boldsymbol{\xi})}{q(\mathbf{x}_T | \mathbf{x}_0, \boldsymbol{\xi})} + \log \prod_{t=2}^T \frac{p_\theta(\mathbf{x}_{t-1} | \mathbf{x}_t)}{q(\mathbf{x}_{t-1} | \mathbf{x}_t, \mathbf{x}_0, \boldsymbol{\xi})} \right] \\
& = \mathbb{E}_{q(\mathbf{x}_{1:T}, \boldsymbol{\xi} | \mathbf{x}_0)} \left[ \log \frac{p(\mathbf{x}_T | \boldsymbol{\xi}) p_\theta(\mathbf{x}_0 | \mathbf{x}_1)}{q(\mathbf{x}_T | \mathbf{x}_0, \boldsymbol{\xi})} + \sum_{t=2}^T \log \frac{p_\theta(\mathbf{x}_{t-1} | \mathbf{x}_t)}{q(\mathbf{x}_{t-1} | \mathbf{x}_t, \mathbf{x}_0, \boldsymbol{\xi})} \right] \\
& = \mathbb{E}_{q(\mathbf{x}_{1:T}, \boldsymbol{\xi} | \mathbf{x}_0)} [\log p_\theta(\mathbf{x}_0 | \mathbf{x}_1)] + \mathbb{E}_{q(\mathbf{x}_{1:T}, \boldsymbol{\xi} | \mathbf{x}_0)} \left[ \log \frac{p(\mathbf{x}_T | \boldsymbol{\xi})}{q(\mathbf{x}_T | \mathbf{x}_0, \boldsymbol{\xi})} \right] + \sum_{t=2}^T \mathbb{E}_{q(\mathbf{x}_{1:T}, \boldsymbol{\xi} | \mathbf{x}_0)} \left[ \log \frac{p_\theta(\mathbf{x}_{t-1} | \mathbf{x}_t)}{q(\mathbf{x}_{t-1} | \mathbf{x}_t, \mathbf{x}_0, \boldsymbol{\xi})} \right] \\
& = \mathbb{E}_{q(\mathbf{x}_1, \boldsymbol{\xi} | \mathbf{x}_0)} [\log p_\theta(\mathbf{x}_0 | \mathbf{x}_1)] + \mathbb{E}_{q(\mathbf{x}_T, \boldsymbol{\xi} | \mathbf{x}_0)} \left[ \log \frac{p(\mathbf{x}_T | \boldsymbol{\xi})}{q(\mathbf{x}_T | \mathbf{x}_0, \boldsymbol{\xi})} \right] + \sum_{t=2}^T \mathbb{E}_{q(\mathbf{x}_t, \mathbf{x}_{t-1}, \boldsymbol{\xi} | \mathbf{x}_0)} \left[ \log \frac{p_\theta(\mathbf{x}_{t-1} | \mathbf{x}_t)}{q(\mathbf{x}_{t-1} | \mathbf{x}_t, \mathbf{x}_0, \boldsymbol{\xi})} \right] \\
& = \mathbb{E}_{q(\boldsymbol{\xi})} \mathbb{E}_{q(\mathbf{x}_1 | \mathbf{x}_0, \boldsymbol{\xi})} [\log p_\theta(\mathbf{x}_0 | \mathbf{x}_1)] + \mathbb{E}_{q(\boldsymbol{\xi})} \mathbb{E}_{q(\mathbf{x}_T | \mathbf{x}_0, \boldsymbol{\xi})} \left[ \log \frac{p(\mathbf{x}_T | \boldsymbol{\xi})}{q(\mathbf{x}_T | \mathbf{x}_0, \boldsymbol{\xi})} \right] \\
& \quad + \sum_{t=2}^T \mathbb{E}_{q(\boldsymbol{\xi})} \mathbb{E}_{q(\mathbf{x}_t | \mathbf{x}_0, \boldsymbol{\xi})} \mathbb{E}_{q(\mathbf{x}_{t-1} | \mathbf{x}_t, \mathbf{x}_0, \boldsymbol{\xi})} \left[ \log \frac{p_\theta(\mathbf{x}_{t-1} | \mathbf{x}_t)}{q(\mathbf{x}_{t-1} | \mathbf{x}_t, \mathbf{x}_0, \boldsymbol{\xi})} \right] \\
& = \mathbb{E}_{q(\boldsymbol{\xi})} \mathbb{E}_{q(\mathbf{x}_1 | \mathbf{x}_0, \boldsymbol{\xi})} [\log p_\theta(\mathbf{x}_0 | \mathbf{x}_1)] - \mathbb{E}_{q(\boldsymbol{\xi})} [D_{\text{KL}}(q(\mathbf{x}_T | \mathbf{x}_0, \boldsymbol{\xi}) || p(\mathbf{x}_T | \boldsymbol{\xi}))] \\
& \quad - \sum_{t=2}^T \mathbb{E}_{q(\boldsymbol{\xi})} \mathbb{E}_{q(\mathbf{x}_t | \mathbf{x}_0, \boldsymbol{\xi})} [D_{\text{KL}}(q(\mathbf{x}_{t-1} | \mathbf{x}_t, \mathbf{x}_0, \boldsymbol{\xi}) || p_\theta(\mathbf{x}_{t-1} | \mathbf{x}_t))]
\end{aligned}$$

### A.2 Derivation of (24)

Suppose that we have  $2T$  random variables  $\{\epsilon_t^*, \epsilon_t\}_{t=0}^{T-1} \stackrel{\text{iid}}{\sim} \mathcal{N}(\epsilon | 0, I)$  and  $\boldsymbol{\xi} \sim q(\boldsymbol{\xi})$ . Then we have for  $t = 1, \dots, T$ :

$$\begin{aligned}
\mathbf{x}_t &= \sqrt{1 - \beta_t} (\mathbf{x}_{t-1} + \gamma_t \boldsymbol{\xi}) + \sqrt{\beta_t} \sigma_0 \epsilon_{t-1} \\
&= \sqrt{\alpha_t} \mathbf{x}_{t-1} + \sqrt{1 - \alpha_t} \sigma_0 \epsilon_{t-1} + \sqrt{\alpha_t} \gamma_t \boldsymbol{\xi} \\
&= \sqrt{\alpha_t} \left( \sqrt{\alpha_{t-1}} \mathbf{x}_{t-2} + \sqrt{1 - \alpha_{t-1}} \sigma_0 \epsilon_{t-2}^* + \sqrt{\alpha_{t-1}} \gamma_{t-1} \boldsymbol{\xi} \right) + \sqrt{1 - \alpha_t} \sigma_0 \epsilon_{t-1} + \sqrt{\alpha_t} \gamma_t \boldsymbol{\xi}
\end{aligned}$$

$$= \sqrt{\alpha_t \alpha_{t-1}} \mathbf{x}_{t-2} + \sqrt{\alpha_t - \alpha_t \alpha_{t-1}} \sigma_0 \boldsymbol{\epsilon}_{t-2}^* + \sqrt{1 - \alpha_t} \sigma_0 \boldsymbol{\epsilon}_{t-1} + (\sqrt{\alpha_t} \gamma_t + \sqrt{\alpha_t \alpha_{t-1}} \gamma_{t-1}) \boldsymbol{\xi} \quad (37)$$

$$= \sqrt{\alpha_t \alpha_{t-1}} \mathbf{x}_{t-2} + \sqrt{1 - \alpha_t \alpha_{t-1}} \sigma_0 \boldsymbol{\epsilon}_{t-2} + (\sqrt{\alpha_t} \gamma_t + \sqrt{\alpha_t \alpha_{t-1}} \gamma_{t-1}) \boldsymbol{\xi} \quad (38)$$

= ...

$$\begin{aligned} &= \sqrt{\prod_{i=1}^t \alpha_i} \mathbf{x}_0 + \sqrt{1 - \prod_{i=1}^t \alpha_i} \sigma_0 \boldsymbol{\epsilon}_0 + \sum_{i=1}^t \sqrt{\prod_{j=i}^t \alpha_j} \gamma_i \boldsymbol{\xi} \\ &= \sqrt{\prod_{i=1}^t \alpha_i} \mathbf{x}_0 + \sqrt{1 - \prod_{i=1}^t \alpha_i} \sigma_0 \boldsymbol{\epsilon}_0 + \sum_{i=1}^t \sqrt{\frac{\prod_{j=0}^t \alpha_j}{\prod_{j=0}^{i-1} \alpha_j}} \gamma_i \boldsymbol{\xi} \\ &= \sqrt{\bar{\alpha}_t} \mathbf{x}_0 + \sqrt{1 - \bar{\alpha}_t} \sigma_0 \boldsymbol{\epsilon}_0 + \sum_{i=1}^t \sqrt{\frac{\bar{\alpha}_t}{\bar{\alpha}_{i-1}}} \gamma_i \boldsymbol{\xi} \\ &= \sqrt{\bar{\alpha}_t} \mathbf{x}_0 + \sqrt{1 - \bar{\alpha}_t} \left( \sigma_0 \boldsymbol{\epsilon}_0 + \frac{1}{\sqrt{1 - \bar{\alpha}_t}} \sum_{i=1}^t \sqrt{\frac{\bar{\alpha}_t}{\bar{\alpha}_{i-1}}} \gamma_i \boldsymbol{\xi} \right) \\ &= \sqrt{\bar{\alpha}_t} \mathbf{x}_0 + \sqrt{1 - \bar{\alpha}_t} (\sigma_0 \boldsymbol{\epsilon}_0 + \boldsymbol{\psi}_t \boldsymbol{\xi}) \end{aligned}$$

See [22] for the transformation from (37) to (38).

### A.3 Derivation of (26)–(29)

For  $t = 2, \dots, T$ , it holds that:

$$\begin{aligned} &q(\mathbf{x}_{t-1} | \mathbf{x}_t, \mathbf{x}_0, \boldsymbol{\xi}) \\ &= \frac{q(\mathbf{x}_t | \mathbf{x}_{t-1}, \mathbf{x}_0, \boldsymbol{\xi}) q(\mathbf{x}_{t-1} | \mathbf{x}_0, \boldsymbol{\xi})}{q(\mathbf{x}_t | \mathbf{x}_0, \boldsymbol{\xi})} \\ &\propto q(\mathbf{x}_t | \mathbf{x}_{t-1}, \mathbf{x}_0, \boldsymbol{\xi}) q(\mathbf{x}_{t-1} | \mathbf{x}_0, \boldsymbol{\xi}) \\ &= \mathcal{N}(\mathbf{x}_t | \sqrt{\bar{\alpha}_t}(\mathbf{x}_{t-1} + \gamma_t \boldsymbol{\xi}), (1 - \alpha_t) \sigma_0^2 I) \mathcal{N}(\mathbf{x}_{t-1} | \sqrt{\bar{\alpha}_{t-1}} \mathbf{x}_0 + \sqrt{1 - \bar{\alpha}_{t-1}} \boldsymbol{\psi}_{t-1} \boldsymbol{\xi}, (1 - \bar{\alpha}_{t-1}) \sigma_0^2 I) \\ &= \mathcal{N}\left(\mathbf{x}_{t-1} \mid \frac{1}{\sqrt{\alpha_t}} \mathbf{x}_t - \gamma_t \boldsymbol{\xi}, \frac{1 - \alpha_t}{\alpha_t} \sigma_0^2 I\right) \mathcal{N}\left(\mathbf{x}_{t-1} \mid \sqrt{\bar{\alpha}_{t-1}} \mathbf{x}_0 + \sqrt{1 - \bar{\alpha}_{t-1}} \boldsymbol{\psi}_{t-1} \boldsymbol{\xi}, (1 - \bar{\alpha}_{t-1}) \sigma_0^2 I\right) \\ &\propto \mathcal{N}\left(\mathbf{x}_{t-1} \mid \tilde{\boldsymbol{\mu}}(\mathbf{x}_t, \mathbf{x}_0, \boldsymbol{\xi}), \tilde{\beta}_t I\right), \end{aligned}$$

where  $\tilde{\boldsymbol{\mu}}(\mathbf{x}_t, \mathbf{x}_0, \boldsymbol{\xi})$  and  $\tilde{\beta}_t$  are given by multiplying two normal distributions as follows:

$$\begin{aligned} \tilde{\boldsymbol{\mu}}(\mathbf{x}_t, \mathbf{x}_0, \boldsymbol{\xi}) &= \frac{1}{\frac{1 - \alpha_t}{\alpha_t} + (1 - \bar{\alpha}_{t-1})} \left( (1 - \bar{\alpha}_{t-1}) \left( \frac{1}{\sqrt{\alpha_t}} \mathbf{x}_t - \gamma_t \boldsymbol{\xi} \right) + \frac{1 - \alpha_t}{\alpha_t} \left( \sqrt{\bar{\alpha}_{t-1}} \mathbf{x}_0 + \sqrt{1 - \bar{\alpha}_{t-1}} \boldsymbol{\psi}_{t-1} \boldsymbol{\xi} \right) \right) \\ &= \frac{\alpha_t}{1 - \bar{\alpha}_t} \left( \frac{1 - \bar{\alpha}_{t-1}}{\sqrt{\alpha_t}} \mathbf{x}_t - (1 - \bar{\alpha}_{t-1}) \gamma_t \boldsymbol{\xi} + \frac{(1 - \alpha_t) \sqrt{\bar{\alpha}_{t-1}}}{\alpha_t} \mathbf{x}_0 + \frac{(1 - \alpha_t) \sqrt{1 - \bar{\alpha}_{t-1}} \boldsymbol{\psi}_{t-1}}{\alpha_t} \boldsymbol{\xi} \right) \\ &= \frac{\sqrt{\alpha_t} (1 - \bar{\alpha}_{t-1})}{1 - \bar{\alpha}_t} \mathbf{x}_t + \frac{(1 - \alpha_t) \sqrt{\bar{\alpha}_{t-1}}}{1 - \bar{\alpha}_t} \mathbf{x}_0 + \frac{(1 - \alpha_t) \sqrt{1 - \bar{\alpha}_{t-1}} \boldsymbol{\psi}_{t-1} - \alpha_t (1 - \bar{\alpha}_{t-1}) \gamma_t}{1 - \bar{\alpha}_t} \boldsymbol{\xi}, \\ &= \frac{\sqrt{\alpha_t} (1 - \bar{\alpha}_{t-1})}{1 - \bar{\alpha}_t} \mathbf{x}_t + \frac{(1 - \alpha_t) \sqrt{\bar{\alpha}_{t-1}}}{1 - \bar{\alpha}_t} \mathbf{x}_0 + \nu_t \boldsymbol{\xi}, \\ \tilde{\beta}_t &= \frac{\frac{1 - \alpha_t}{\alpha_t} \sigma_0^2 (1 - \bar{\alpha}_{t-1}) \sigma_0^2}{\frac{1 - \alpha_t}{\alpha_t} \sigma_0^2 + (1 - \bar{\alpha}_{t-1}) \sigma_0^2} = \frac{(1 - \alpha_t) (1 - \bar{\alpha}_{t-1})}{1 - \bar{\alpha}_t} \sigma_0^2 \end{aligned}$$

## A.4 Proof of Lemma 3.3

From (24), we have

$$\mathbf{x}_0 = \frac{1}{\sqrt{\bar{\alpha}_t}} \left( \mathbf{x}_t - \sqrt{1 - \bar{\alpha}_t} (\sigma_0 \boldsymbol{\epsilon}_0 + \psi_t \boldsymbol{\xi}) \right)$$

By substituting this into (27), we obtain

$$\begin{aligned} \tilde{\mu}(\mathbf{x}_t, \mathbf{x}_0, \boldsymbol{\xi}) &= \frac{\sqrt{\bar{\alpha}_t}(1 - \bar{\alpha}_{t-1})}{1 - \bar{\alpha}_t} \mathbf{x}_t + \frac{(1 - \alpha_t)\sqrt{\bar{\alpha}_{t-1}}}{1 - \bar{\alpha}_t} \frac{1}{\sqrt{\bar{\alpha}_t}} \left( \mathbf{x}_t - \sqrt{1 - \bar{\alpha}_t} (\sigma_0 \boldsymbol{\epsilon}_0 + \psi_t \boldsymbol{\xi}) \right) + \nu_t \boldsymbol{\xi} \\ &= \frac{1}{\sqrt{\bar{\alpha}_t}} \mathbf{x}_t - \frac{1 - \alpha_t}{\sqrt{1 - \bar{\alpha}_t} \sqrt{\bar{\alpha}_t}} \left( \sigma_0 \boldsymbol{\epsilon}_0 + \left( \psi_t - \frac{\sqrt{1 - \bar{\alpha}_t} \sqrt{\bar{\alpha}_t}}{1 - \alpha_t} \nu_t \right) \boldsymbol{\xi} \right) \\ &= \frac{1}{\sqrt{\bar{\alpha}_t}} \mathbf{x}_t - \frac{1 - \alpha_t}{\sqrt{1 - \bar{\alpha}_t} \sqrt{\bar{\alpha}_t}} (\sigma_0 \boldsymbol{\epsilon}_0 + \phi_t \boldsymbol{\xi}), \end{aligned}$$

where  $\phi_t = \psi_t - \frac{\sqrt{1 - \bar{\alpha}_t} \sqrt{\bar{\alpha}_t}}{1 - \alpha_t} \nu_t$ . We can expand  $\phi_t$  as follows:

$$\begin{aligned} \phi_t &= \psi_t - \frac{\sqrt{1 - \bar{\alpha}_t} \sqrt{\bar{\alpha}_t}}{1 - \alpha_t} \nu_t \\ &= \psi_t - \frac{\sqrt{1 - \bar{\alpha}_t} \sqrt{\bar{\alpha}_t} (1 - \alpha_t) \sqrt{1 - \bar{\alpha}_{t-1}} \psi_{t-1} - \alpha_t (1 - \bar{\alpha}_{t-1}) \gamma_t}{1 - \alpha_t (1 - \bar{\alpha}_{t-1})} \\ &= \psi_t - \frac{\sqrt{1 - \bar{\alpha}_{t-1}} \sqrt{\bar{\alpha}_t}}{\sqrt{1 - \bar{\alpha}_t}} \psi_{t-1} + \frac{\alpha_t \sqrt{\bar{\alpha}_t} (1 - \bar{\alpha}_{t-1})}{(1 - \alpha_t) \sqrt{1 - \bar{\alpha}_t}} \gamma_t \end{aligned} \tag{39}$$

From the definition of  $\psi_t$ , we find that

$$\psi_t = \frac{\sqrt{\bar{\alpha}_t} \sqrt{1 - \bar{\alpha}_{t-1}}}{\sqrt{1 - \bar{\alpha}_t}} \psi_{t-1} + \frac{\sqrt{\bar{\alpha}_t}}{\sqrt{1 - \bar{\alpha}_t}} \gamma_t, \tag{40}$$

Then, by substituting (40) into (39), we get

$$\begin{aligned} \phi_t &= \frac{\sqrt{\bar{\alpha}_t} \sqrt{1 - \bar{\alpha}_{t-1}}}{\sqrt{1 - \bar{\alpha}_t}} \psi_{t-1} + \frac{\sqrt{\bar{\alpha}_t}}{\sqrt{1 - \bar{\alpha}_t}} \gamma_t - \frac{\sqrt{1 - \bar{\alpha}_{t-1}} \sqrt{\bar{\alpha}_t}}{\sqrt{1 - \bar{\alpha}_t}} \psi_{t-1} + \frac{\alpha_t \sqrt{\bar{\alpha}_t} (1 - \bar{\alpha}_{t-1})}{(1 - \alpha_t) \sqrt{1 - \bar{\alpha}_t}} \gamma_t \\ &= \frac{\sqrt{\bar{\alpha}_t} (1 - \alpha_t) + \alpha_t \sqrt{\bar{\alpha}_t} (1 - \bar{\alpha}_{t-1})}{(1 - \alpha_t) \sqrt{1 - \bar{\alpha}_t}} \gamma_t \\ &= \frac{\sqrt{\bar{\alpha}_t} (1 - \bar{\alpha}_t)}{(1 - \alpha_t) \sqrt{1 - \bar{\alpha}_t}} \gamma_t \\ &= \frac{\sqrt{\bar{\alpha}_t} \sqrt{1 - \bar{\alpha}_t}}{1 - \alpha_t} \gamma_t \end{aligned}$$

## A.5 Derivation of (32)

With respect to  $\mathcal{L}_1$ , from (24) with  $t = 1$ , we have

$$\begin{aligned} &\mathbb{E}_{q(\mathbf{x}_1 | \mathbf{x}_0, \boldsymbol{\xi})} [\log p_\theta(\mathbf{x}_0 | \mathbf{x}_1)] \\ &= \mathbb{E}_{q(\mathbf{x}_1 | \mathbf{x}_0, \boldsymbol{\xi})} [\log \mathcal{N}(\mathbf{x}_0 | \mu_\theta(\mathbf{x}_1, 1), \sigma_1^2 I)] \\ &= -\frac{1}{2\sigma_1^2} \mathbb{E}_{q(\mathbf{x}_1 | \mathbf{x}_0, \boldsymbol{\xi})} [\|\mathbf{x}_0 - \mu_\theta(\mathbf{x}_1, 1)\|^2] + C_2 \\ &= -\frac{1}{2\sigma_1^2} \mathbb{E}_{q(\mathbf{x}_1 | \mathbf{x}_0, \boldsymbol{\xi})} \left[ \left\| \mathbf{x}_0 - \left( \frac{1}{\sqrt{\alpha_1}} \mathbf{x}_1 - \frac{1 - \alpha_1}{\sqrt{1 - \bar{\alpha}_1} \sqrt{\alpha_1}} \boldsymbol{\epsilon}_\theta(\mathbf{x}_1, 1) \right) \right\|^2 \right] + C_2 \end{aligned}$$

$$\begin{aligned}
&= -\frac{1}{2\sigma_1^2} \mathbb{E}_{\mathcal{N}(\epsilon_0|0,I)} \left[ \left\| \mathbf{x}_0 - \left( \frac{1}{\sqrt{\alpha_1}} (\sqrt{\alpha_1} \mathbf{x}_0 + \sqrt{1-\alpha_1} (\sigma_0 \epsilon_0 + \psi_1 \boldsymbol{\xi})) - \frac{\sqrt{1-\alpha_1}}{\sqrt{\alpha_1}} \epsilon_\theta(\mathbf{x}_1, 1) \right) \right\|^2 \right] + C_2 \\
&= -\frac{1}{2\sigma_1^2} \mathbb{E}_{\mathcal{N}(\epsilon_0|0,I)} \left[ \left\| \frac{\sqrt{1-\alpha_1}}{\sqrt{\alpha_1}} (\sigma_0 \epsilon_0 + \psi_1 \boldsymbol{\xi} - \epsilon_\theta(\mathbf{x}_1, 1)) \right\|^2 \right] + C_2 \\
&= -\frac{1-\alpha_1}{2\sigma_1^2 \alpha_1} \mathbb{E}_{\mathcal{N}(\epsilon_0|0,I)} \left[ \|\sigma_0 \epsilon_0 + \psi_1 \boldsymbol{\xi} - \epsilon_\theta(\mathbf{x}_1, 1)\|^2 \right] + C_2 \\
&= -\frac{1-\alpha_1}{2\sigma_1^2 \alpha_1} \mathbb{E}_{\mathcal{N}(\epsilon_0|0,I)} \left[ \|\sigma_0 \epsilon_0 + \phi_1 \boldsymbol{\xi} - \epsilon_\theta(\mathbf{x}_1, 1)\|^2 \right] + C_2 \\
&= -\lambda_1 \mathbb{E}_{\mathcal{N}(\epsilon_0|0,I)} \left[ \|\sigma_0 \epsilon_0 + \phi_1 \boldsymbol{\xi} - \epsilon_\theta(\mathbf{x}_1, 1)\|^2 \right] + C_2
\end{aligned}$$

## A.6 Proof of Proposition 5.1

Following [27], from (24), we have

$$\begin{aligned}
\mathbf{x}_0 &= \sqrt{\bar{\alpha}_t} \mathbf{x}_t - \sqrt{1-\bar{\alpha}_t} \mathbf{v}_t, \\
\mathbf{v}_t &= \sqrt{\bar{\alpha}_t} (\sigma_0 \epsilon_0 + \psi_t \boldsymbol{\xi}) - \sqrt{1-\bar{\alpha}_t} \mathbf{x}_0,
\end{aligned} \tag{41}$$

where  $\mathbf{v}_t = \frac{d\mathbf{x}_t}{d\omega_t}$  and  $\omega_t$  is the angle satisfying  $\cos(\omega_t) = \sqrt{\bar{\alpha}_t}$ ,  $\sin(\omega_t) = \sqrt{1-\bar{\alpha}_t}$ . By substituting (41) into (27), we obtain

$$\begin{aligned}
\tilde{\mu}(\mathbf{x}_t, \mathbf{x}_0, \boldsymbol{\xi}) &= \frac{\sqrt{\alpha_t}(1-\bar{\alpha}_{t-1})}{1-\bar{\alpha}_t} \mathbf{x}_t + \frac{(1-\alpha_t)\sqrt{\bar{\alpha}_{t-1}}}{1-\bar{\alpha}_t} (\sqrt{\bar{\alpha}_t} \mathbf{x}_t - \sqrt{1-\bar{\alpha}_t} \mathbf{v}_t) + \nu_t \boldsymbol{\xi} \\
&= \frac{\sqrt{\alpha_t}(1-\bar{\alpha}_{t-1}) + (1-\alpha_t)\sqrt{\bar{\alpha}_{t-1}\bar{\alpha}_t}}{1-\bar{\alpha}_t} \mathbf{x}_t - \frac{(1-\alpha_t)\sqrt{\bar{\alpha}_{t-1}}}{\sqrt{1-\bar{\alpha}_t}} \left( \mathbf{v}_t - \frac{\sqrt{1-\bar{\alpha}_t}}{(1-\alpha_t)\sqrt{\bar{\alpha}_{t-1}}} \nu_t \boldsymbol{\xi} \right)
\end{aligned}$$

Since  $\nu_t = 0$  under the balanced- $\phi_t, \psi_t$  strategy, we obtain

$$\begin{aligned}
\tilde{\mu}(\mathbf{x}_t, \mathbf{x}_0, \boldsymbol{\xi}) &= \frac{\sqrt{\alpha_t}(1-\bar{\alpha}_{t-1}) + (1-\alpha_t)\sqrt{\bar{\alpha}_{t-1}\bar{\alpha}_t}}{1-\bar{\alpha}_t} \mathbf{x}_t - \frac{(1-\alpha_t)\sqrt{\bar{\alpha}_{t-1}}}{\sqrt{1-\bar{\alpha}_t}} \mathbf{v}_t \\
&= \frac{\sqrt{\alpha_t}(1-\bar{\alpha}_{t-1}) + (1-\alpha_t)\sqrt{\bar{\alpha}_{t-1}\bar{\alpha}_t}}{1-\bar{\alpha}_t} \mathbf{x}_t - \frac{(1-\alpha_t)\sqrt{\bar{\alpha}_{t-1}}}{\sqrt{1-\bar{\alpha}_t}} (\sqrt{\bar{\alpha}_t} (\sigma_0 \epsilon_0 + \psi_t \boldsymbol{\xi}) - \sqrt{1-\bar{\alpha}_t} \mathbf{x}_0)
\end{aligned}$$

Therefore, if we parametrize  $\mu_\theta(\mathbf{x}_t, t)$  by

$$\mu_\theta(\mathbf{x}_t, t) = \frac{\sqrt{\alpha_t}(1-\bar{\alpha}_{t-1}) + (1-\alpha_t)\sqrt{\bar{\alpha}_{t-1}\bar{\alpha}_t}}{1-\bar{\alpha}_t} \mathbf{x}_t - \frac{(1-\alpha_t)\sqrt{\bar{\alpha}_{t-1}}}{\sqrt{1-\bar{\alpha}_t}} v_\theta(\mathbf{x}_t, t),$$

then, the KL divergence in  $\mathcal{L}_3$  can be transformed as follows for  $t = 2, \dots, T$ :

$$\begin{aligned}
&D_{\text{KL}}(q(\mathbf{x}_{t-1}|\mathbf{x}_t, \mathbf{x}_0, \boldsymbol{\xi}) \parallel p_\theta(\mathbf{x}_{t-1}|\mathbf{x}_t)) \\
&= \frac{1}{2\sigma_t^2} \mathbb{E}_{q(\mathbf{x}_{t-1}|\mathbf{x}_t, \mathbf{x}_0, \boldsymbol{\xi})} \left[ \|\tilde{\mu}(\mathbf{x}_t, \mathbf{x}_0, \boldsymbol{\xi}) - \mu_\theta(\mathbf{x}_t, t)\|^2 \right] + C_1 \\
&= \frac{\bar{\alpha}_{t-1}(1-\alpha_t)^2}{2\sigma_t^2(1-\bar{\alpha}_t)} \mathbb{E}_{\mathcal{N}(\epsilon_0|0,I)} \left[ \|\sqrt{\bar{\alpha}_t} (\sigma_0 \epsilon_0 + \psi_t \boldsymbol{\xi}) - \sqrt{1-\bar{\alpha}_t} \mathbf{x}_0 - v_\theta(\mathbf{x}_t, t)\|^2 \right] + C_3,
\end{aligned}$$

where  $C_3$  is a constant that does not depend on  $\theta$ .

With respect to  $\mathcal{L}_1$  in (23), we have

$$\begin{aligned}
&\mathbb{E}_{q(\mathbf{x}_1|\mathbf{x}_0, \boldsymbol{\xi})} [\log p_\theta(\mathbf{x}_0|\mathbf{x}_1)] \\
&= \mathbb{E}_{q(\mathbf{x}_1|\mathbf{x}_0, \boldsymbol{\xi})} [\log \mathcal{N}(\mathbf{x}_0 \mid \mu_\theta(\mathbf{x}_1, 1), \sigma_1^2 I)]
\end{aligned}$$

$$\begin{aligned}
&= -\frac{1}{2\sigma_1^2} \mathbb{E}_{q(\mathbf{x}_1|\mathbf{x}_0, \boldsymbol{\xi})} \left[ \|\mathbf{x}_0 - \mu_\theta(\mathbf{x}_1, 1)\|^2 \right] + C_2 \\
&= -\frac{1}{2\sigma_1^2} \mathbb{E}_{q(\mathbf{x}_1|\mathbf{x}_0, \boldsymbol{\xi})} \left[ \left\| \mathbf{x}_0 - \frac{\sqrt{\alpha_1}(1 - \bar{\alpha}_0) + (1 - \alpha_1)\sqrt{\bar{\alpha}_0\bar{\alpha}_1}}{1 - \bar{\alpha}_1} \mathbf{x}_1 + \frac{(1 - \alpha_1)\sqrt{\bar{\alpha}_0}}{\sqrt{1 - \bar{\alpha}_1}} v_\theta(\mathbf{x}_1, 1) \right\|^2 \right] + C_2 \\
&= -\frac{1}{2\sigma_1^2} \mathbb{E}_{q(\mathbf{x}_1|\mathbf{x}_0, \boldsymbol{\xi})} \left[ \|\mathbf{x}_0 - \sqrt{\alpha_1} \mathbf{x}_1 + \sqrt{1 - \alpha_1} v_\theta(\mathbf{x}_1, 1)\|^2 \right] + C_2 \\
&= -\frac{1}{2\sigma_1^2} \mathbb{E}_{q(\mathbf{x}_1|\mathbf{x}_0, \boldsymbol{\xi})} \left[ \|\sqrt{1 - \alpha_1} \mathbf{v}_1 + \sqrt{1 - \alpha_1} v_\theta(\mathbf{x}_1, 1)\|^2 \right] + C_2 \\
&= -\frac{1 - \alpha_1}{2\sigma_1^2} \mathbb{E}_{q(\mathbf{x}_1|\mathbf{x}_0, \boldsymbol{\xi})} \left[ \|\mathbf{v}_1 - v_\theta(\mathbf{x}_1, 1)\|^2 \right] + C_2 \\
&= -\frac{1 - \alpha_1}{2\sigma_1^2} \mathbb{E}_{\mathcal{N}(\boldsymbol{\epsilon}_0|0, I)} \left[ \|\sqrt{\alpha_1}(\sigma_0 \boldsymbol{\epsilon}_0 + \boldsymbol{\psi}_1 \boldsymbol{\xi}) - \sqrt{1 - \alpha_1} \mathbf{x}_0 - v_\theta(\mathbf{x}_1, 1)\|^2 \right] + C_2
\end{aligned}$$

Therefore, under the balanced- $\phi_t, \psi_t$  strategy, the training loss for maximizing the evidence lower bound in (23) with respect to  $\theta$  under the  $v$ -prediction formulation is

$$\ell^v(\theta) = \mathbb{E}_{q(\boldsymbol{\xi}), \mathcal{U}(t|1, T), \mathcal{N}(\boldsymbol{\epsilon}_0|0, I)} \left[ \frac{\bar{\alpha}_{t-1}(1 - \alpha_t)^2}{2\sigma_t^2(1 - \bar{\alpha}_t)} \|\sqrt{\bar{\alpha}_t}(\sigma_0 \boldsymbol{\epsilon}_0 + \boldsymbol{\psi}_t \boldsymbol{\xi}) - \sqrt{1 - \bar{\alpha}_t} \mathbf{x}_0 - v_\theta(\mathbf{x}_t, t)\|^2 \right],$$

where  $\mathbf{x}_t$  is given by (24).

## B Python code for generating the Cylinder dataset

Figure 6 shows the Python code for generating the Cylinder dataset.

## C Additional experimental results

### C.1 Training with data scaling

The Base model was trained on the Cylinder dataset with dimensionality  $n = 200$  by using data scaling with a scaling parameter  $\rho$ . Specifically,  $\rho$  was set to one of 0.7, 0.8, 0.9, 1.1, 1.2, or 1.3 (note that  $\rho = 1.0$  corresponds to the case without data scaling). The values of 1WD and MMD during training for each configuration are shown in Figure 7. For comparison, the results for the Base model without data scaling ( $\rho = 1.0$ ) and the Proposed model ( $\sigma_c^2 = 1.0$ ) are also included in the figure. It can be seen that applying data scaling with  $\rho = 1.1$  to the Base model results in smaller 1WD and MMD values compared to the case without scaling ( $\rho = 1.0$ ). However, the Proposed model achieves even smaller 1WD and MMD values.

Next, using each Base model trained with data scaling, we generated 5000 data points and compared the distribution of their average brightness  $L_{\text{avg}}(\mathbf{x}_0)$  with that of the test dataset. The results are shown in Figure 8. From the figure, it can be seen that applying data scaling to the Cylinder dataset ( $n = 200$ ) does not significantly change the distribution of  $L_{\text{avg}}(\mathbf{x}_0)$  in the generated outputs. This suggests that simply applying data scaling in the Base model does not resolve the difficulty in generating data with extreme average brightness.

#### C.1.1 Comparison of average brightness distributions for $v$ -prediction models

The distributions of  $L_{\text{avg}}(\mathbf{x}_0)$  for data generated by each  $v$ -prediction model are compared with that of the test dataset in Figure 9. The results for the Base model, the Offset noise model ( $\sigma_c^2 = 0.1$ ), and the Proposed model ( $\sigma_c^2 = 1.0$ ) are presented in the top, middle, and bottom rows, respectively, for each  $n$ . The models used were those obtained after the final training step of 200,000 for each setting.

```

1 import torch
2
3 def cylinder_dataset(size: int, dim: int, r: float = 0.5, top_center: float = 2.0):
4     """
5     Generate a cylinder-shaped dataset in n-dimensional space.
6
7     Args:
8         size: Number of samples to generate.
9         dim: Dimensionality of the space.
10        r: Radius of the cylinder (relative to the norm of a vector of ones).
11        top_center: The center of the top of the cylinder.
12
13    Returns:
14        Tensor containing the generated cylinder dataset.
15    """
16
17    # Create a vector of all ones, which will define the cylinder's axis direction.
18    vec_ones = torch.ones(dim)
19
20    # Adjust the radius relative to the dimensionality using L2 norm.
21    adjusted_r = r * vec_ones.norm(p=2)
22
23    # Generate random unit vectors orthogonal to vec_ones (the cylinder's axis).
24    vec_ortho = torch.randn(size, dim)
25    vec_ortho = vec_ortho - vec_ortho.mm(vec_ones[:, None]) / dim * vec_ones
26    vec_ortho = vec_ortho / vec_ortho.norm(p=2, dim=1)[:, None]
27
28    # Scale the orthogonal vectors by random radii within the cylinder's radius.
29    vec_ortho = vec_ortho * torch.rand(size).mul(adjusted_r)[:, None]
30
31    # Scale vec_ones to random heights within [-top_center, top_center].
32    vec_ones = vec_ones * torch.rand(size).mul(2 * top_center).sub(top_center)[:, None]
33
34    # Combine the axis and orthogonal components to form the final dataset.
35    data = vec_ones + vec_ortho
36
37    return data
38

```

Figure 6: Python code for generating the Cylinder dataset.

## References

- [1] Jacob Austin, Daniel D Johnson, Jonathan Ho, Daniel Tarlow, and Rianne Van Den Berg. Structured denoising diffusion models in discrete state-spaces. *Advances in Neural Information Processing Systems*, 2021.
- [2] Tianrong Chen, Guan-Horng Liu, and Evangelos Theodorou. Likelihood training of Schrödinger bridge using forward-backward sdes theory. In *International Conference on Learning Representations*, 2022.
- [3] Gabriele Corso, Bowen Jing, Regina Barzilay, Tommi Jaakkola, et al. Diffdock: Diffusion steps, twists, and turns for molecular docking. In *International Conference on Learning Representations*, 2023.
- [4] Valentin De Bortoli, James Thornton, Jeremy Heng, and Arnaud Doucet. Diffusion Schrödinger bridge with applications to score-based generative modeling. *Advances in Neural Information Processing Systems*, 34:17695–17709, 2021.
- [5] Prafulla Dhariwal and Alexander Nichol. Diffusion models beat GANs on image synthesis. *Advances in neural information processing systems*, 34:8780–8794, 2021.
- [6] Ian Goodfellow, Jean Pouget-Abadie, Mehdi Mirza, Bing Xu, David Warde-Farley, Sherjil Ozair, Aaron Courville, and Yoshua Bengio. Generative adversarial nets. *Advances in neural information processing systems*, 27, 2014.
- [7] Arthur Gretton, Karsten M Borgwardt, Malte J Rasch, Bernhard Schölkopf, and Alexander Smola. A kernel two-sample test. *Journal of Machine Learning Research*, 13(1):723–773, 2012.

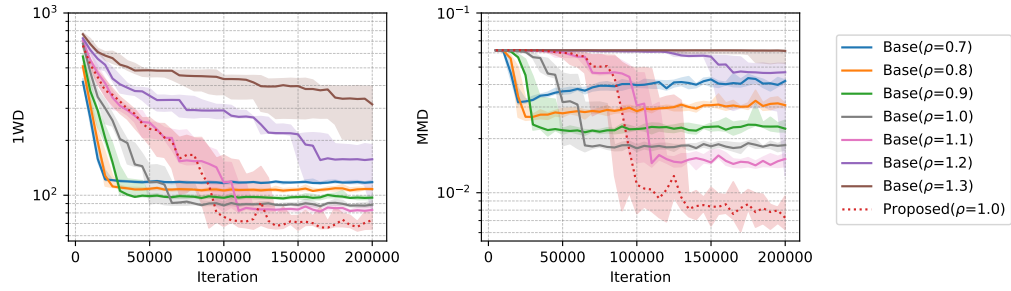


Figure 7: Changes in 1WD and MMD during the training of the Base model ( $n = 200$ ) with data scaling using various scaling parameters  $\rho$ . For comparison, the results of the proposed model without data scaling ( $\rho = 1.0$ ) and the Proposed model ( $\sigma_c^2 = 1.0$ ) are also included.

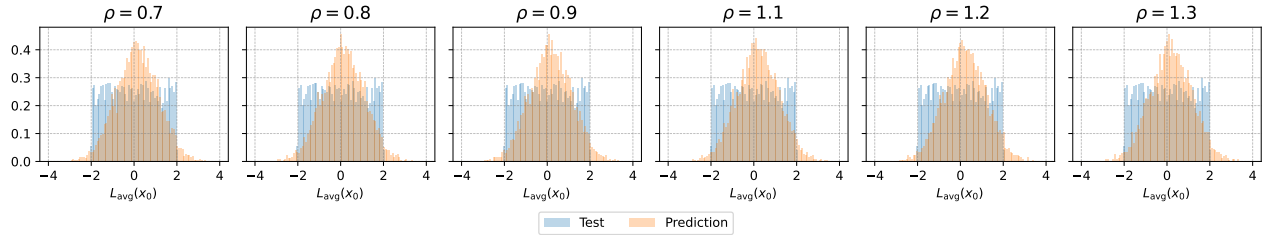


Figure 8: Comparison of average brightness  $L_{\text{avg}}(\mathbf{x}_0)$  distributions of the Base model ( $n = 200$ ) with data scaling using various scaling parameters  $\rho$ .

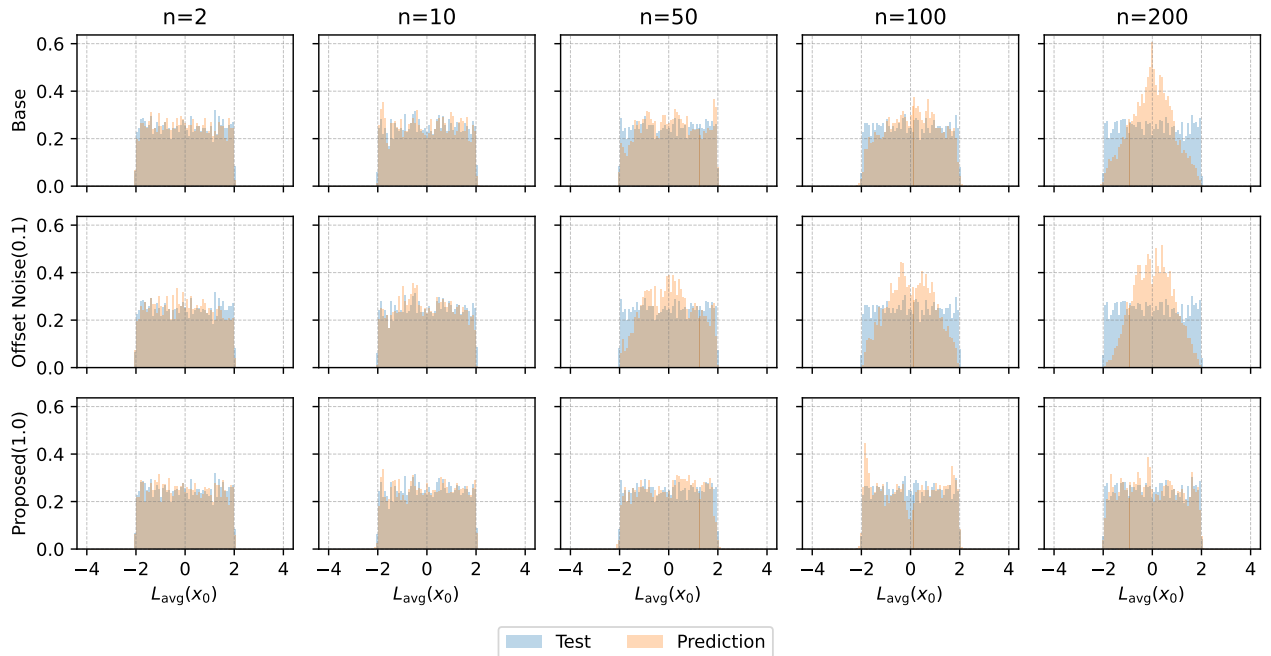


Figure 9: Comparison of distributions of average brightness  $L_{\text{avg}}(\mathbf{x}_0)$  between the test data and the generated data using  $v$ -prediction models.

- [8] Jiaqi Guan, Xiangxin Zhou, Yuwei Yang, Yu Bao, Jian Peng, Jianzhu Ma, Qiang Liu, Liang Wang, and Quanquan Gu. Decompdiff: Diffusion models with decomposed priors for structure-based drug design. In *International Conference on Machine Learning*, 2023.
- [9] Nicholas Guttenberg. Diffusion with offset noise. <https://www.crosslabs.org/blog/diffusion-with-offset-noise> (Accessed 2024/08/30).
- [10] Dan Hendrycks and Kevin Gimpel. Gaussian error linear units (GELUs), 2016.
- [11] Jonathan Ho, Ajay Jain, and Pieter Abbeel. Denoising diffusion probabilistic models. *Advances in neural information processing systems*, 33:6840–6851, 2020.
- [12] Minghui Hu, Jianbin Zheng, Chuanxia Zheng, Chaoyue Wang, Dacheng Tao, and Tat-Jen Cham. One more step: A versatile plug-and-play module for rectifying diffusion schedule flaws and enhancing low-frequency controls. In *Proceedings of the IEEE/CVF Conference on Computer Vision and Pattern Recognition*, pages 7331–7340, 2024.
- [13] Illuminati Diffusion Development Team. Illuminati diffusion v1.1, 2023. URL <https://civitai.com/models/11193/illuminati-diffusion-v11>.
- [14] Tero Karras, Miika Aittala, Timo Aila, and Samuli Laine. Elucidating the design space of diffusion-based generative models. *Advances in neural information processing systems*, 35:26565–26577, 2022.
- [15] Diederik P Kingma. Auto-encoding variational bayes. *arXiv preprint arXiv:1312.6114*, 2013.
- [16] Diederik P Kingma and Jimmy Ba. Adam: A method for stochastic optimization. In *International Conference on Learning Representations*, 2015.
- [17] Zhifeng Kong, Wei Ping, Jiaji Huang, Kexin Zhao, and Bryan Catanzaro. Diffwave: A versatile diffusion model for audio synthesis. In *International Conference on Learning Representations*, 2021.
- [18] Xiang Li, John Thickstun, Ishaan Gulrajani, Percy S Liang, and Tatsunori B Hashimoto. Diffusion-lm improves controllable text generation. *Advances in Neural Information Processing Systems*, 2022.
- [19] Shanchuan Lin, Bingchen Liu, Jiashi Li, and Xiao Yang. Common diffusion noise schedules and sample steps are flawed. In *Proceedings of the IEEE/CVF winter conference on applications of computer vision*, pages 5404–5411, 2024.
- [20] Guan-Horng Liu, Arash Vahdat, De-An Huang, Evangelos Theodorou, Weili Nie, and Anima Anandkumar. I<sup>2</sup>SB: Image-to-image Schrödinger bridge. In *International Conference on Machine Learning*, pages 22042–22062. PMLR, 2023.
- [21] Kingchao Liu, Chengyue Gong, et al. Flow straight and fast: Learning to generate and transfer data with rectified flow. In *International Conference on Learning Representations*, 2023.
- [22] Calvin Luo. Understanding diffusion models: A unified perspective. *arXiv preprint arXiv:2208.11970*, 2022.
- [23] Razvan Pascanu, Tomas Mikolov, and Yoshua Bengio. On the difficulty of training recurrent neural networks. In *International Conference on Machine Learning*, 2013.
- [24] Frank Permenter and Chenyang Yuan. Interpreting and improving diffusion models from an optimization perspective. In *International Conference on Machine Learning*, 2024.
- [25] Dustin Podell, Zion English, Kyle Lacey, Andreas Blattmann, Tim Dockhorn, Jonas Müller, Joe Penna, and Robin Rombach. SDXL: Improving latent diffusion models for high-resolution image synthesis. In *The Twelfth International Conference on Learning Representations*, 2024.

- [26] Robin Rombach, Andreas Blattmann, Dominik Lorenz, Patrick Esser, and Björn Ommer. High-resolution image synthesis with latent diffusion models. In *Proceedings of the IEEE/CVF conference on computer vision and pattern recognition*, pages 10684–10695, 2022.
- [27] Tim Salimans and Jonathan Ho. Progressive distillation for fast sampling of diffusion models. *arXiv preprint arXiv:2202.00512*, 2022.
- [28] Jascha Sohl-Dickstein, Eric Weiss, Niru Maheswaranathan, and Surya Ganguli. Deep unsupervised learning using nonequilibrium thermodynamics. In *International conference on machine learning*, pages 2256–2265. PMLR, 2015.
- [29] Yang Song, Jascha Sohl-Dickstein, Diederik P Kingma, Abhishek Kumar, Stefano Ermon, and Ben Poole. Score-based generative modeling through stochastic differential equations. In *International Conference on Learning Representations*, 2021.
- [30] Stability AI. Stable diffusion v2, 2022. URL <https://huggingface.co/stabilityai/stable-diffusion-2>.
- [31] Alexander Tong, Kilian FATRAS, Nikolay Malkin, Guillaume Huguët, Yanlei Zhang, Jarrid Rector-Brooks, Guy Wolf, and Yoshua Bengio. Improving and generalizing flow-based generative models with minibatch optimal transport. *Transactions on Machine Learning Research*, 2024. ISSN 2835-8856.
- [32] Cédric Villani. *Optimal Transport: Old and New*. Grundlehren der mathematischen Wissenschaften. Springer Berlin Heidelberg, 2008. ISBN 9783540710509.
- [33] Jonathan Whitaker. Multi-resolution noise for diffusion model training, 2023. URL [https://wandb.ai/johnowhitaker/multires\\_noise/reports/Multi-Resolution-Noise-for-Diffusion-Model-Training--VmlldzozNjYyOTU2](https://wandb.ai/johnowhitaker/multires_noise/reports/Multi-Resolution-Noise-for-Diffusion-Model-Training--VmlldzozNjYyOTU2).